JACS
JOURNAL OF THE AMERICAN CHEMICAL SOCIETY

Made available for a limited time for personal research and study only License.

pubs.acs.org/JACS

Communication

Single-molecule Detection of Ultrafast Biomolecular Dynamics with Nanophotonics

Mark F. Nüesch, Miloš T. Ivanović, Jean-Benoît Claude, Daniel Nettels, Robert B. Best,* Jérôme Wenger,* and Benjamin Schuler*

Cite This: J. Am. Chem. Soc. 2022, 144, 52−56

Read Online

ACCESS | Metrics & More | Article Recommendations | Supporting Information

ABSTRACT: Single-molecule Förster resonance energy transfer (FRET) is a versatile technique for probing the structure and dynamics of biomolecules even in heterogeneous ensembles. However, because of the limited fluorescence brightness per molecule and the relatively long fluorescence lifetimes, probing ultrafast structural dynamics in the nanosecond time scale has thus far been very challenging. Here, we demonstrate that nanophotonic fluorescence enhancement in zero-mode waveguides enables measurements of previously inaccessible low-nanosecond dynamics by dramatically improving time resolution and reduces data acquisition times by more than an order of magnitude. As a prototypical example, we use this approach to probe the dynamics of a short intrinsically disordered peptide that were previously inaccessible with single-molecule FRET measurements. We show that we are now able to detect the low-nanosecond correlations in this peptide, and we obtain a detailed interpretation of the underlying distance distributions and dynamics in conjunction with all-atom molecular dynamics simulations, which agree remarkably well with the experiments. We expect this combined approach to be widely applicable to the investigation of very rapid biomolecular dynamics.

Investigating the entire spectrum of biomolecular dynamics is essential for understanding the mechanisms of biological processes at the molecular scale. A powerful class of methods for probing a broad range of time scales is single-molecule fluorescence spectroscopy.[1−8] The application of single-molecule Förster resonance energy transfer (FRET), *e.g.*, is particularly common for obtaining information on molecular distances and dynamics from milliseconds to minutes. However, monitoring more rapid intramolecular distance dynamics often remains a challenge.

Time scales down to the submicrosecond regime can be reached with fluorescence correlation spectroscopy[2] (FCS) combined with single-molecule FRET between a donor and acceptor fluorophore attached to specific sites on biomolecules.[3,4] One important application of this nanosecond fluorescence correlation spectroscopy (nsFCS) has been the investigation of the rapid chain dynamics of unfolded polypeptides and intrinsically disordered proteins.[10,11] By globally analyzing the donor−donor, acceptor−acceptor, and donor−acceptor fluorescence intensity correlations, distance dynamics can be quantified and distinguished from other contributions such as fluorescence quenching or rotational motion.[11,12] Moreover, subpopulations can be separated and their dynamics extracted even for heterogeneous mixtures of conformational states.[3,4,10] Disordered proteins of 50−100 residues typically exhibit chain reconfiguration times of tens to hundreds of nanoseconds.[11]

However, nsFCS currently suffers from two major limitations. First, data acquisition times of 10 h or more are often required for reliably quantifying dynamics in the submicrosecond regime, which limits sample throughput. Given typical photon count rates below 10^6 s^{-1}, the probability of detecting photons separated by nanoseconds, the key requirement for retrieving information on this time scale, is intrinsically low. Second, the shortest accessible times are limited by the fluorescence lifetimes of the fluorophores, typically a few nanoseconds. If the distance dynamics of interest are not well separated from this range, distinguishing the two contributions becomes difficult and has limited the use of nsFCS to distance dynamics above ∼20 ns.[11]

Here we use nanophotonics in zero-mode waveguides (ZMWs) to overcome these limitations. ZMWs are subwavelength apertures (Figure 1a, Supporting Information (SI), Figure S1) that were first introduced as a means of reducing the observation volume to the attoliter range and thus enabling single-molecule detection at much higher concentrations than previously possible.[13,14] However, another major advantage of ZMWs for single-molecule spectroscopy is the enhancement of fluorescence emission by the local environment in the nanocavity:[15−17] The fluorescence brightness is increased, which improves the signal-to-noise ratio and reduces data acquisition times. Simultaneously, fluorescence lifetimes are decreased, which enables access to a broader range of dynamics in the nanosecond regime.

Figure 1 shows the effect of ZMWs produced by focused ion-beam milling in a 100 nm aluminum layer on the confocal single-molecule detection of the commonly used Alexa Fluors 488 and

Received: September 4, 2021
Published: December 31, 2021

ACS Publications

© 2021 American Chemical Society

https://doi.org/10.1021/jacs.1c09387
J. Am. Chem. Soc. 2022, 144, 52−56

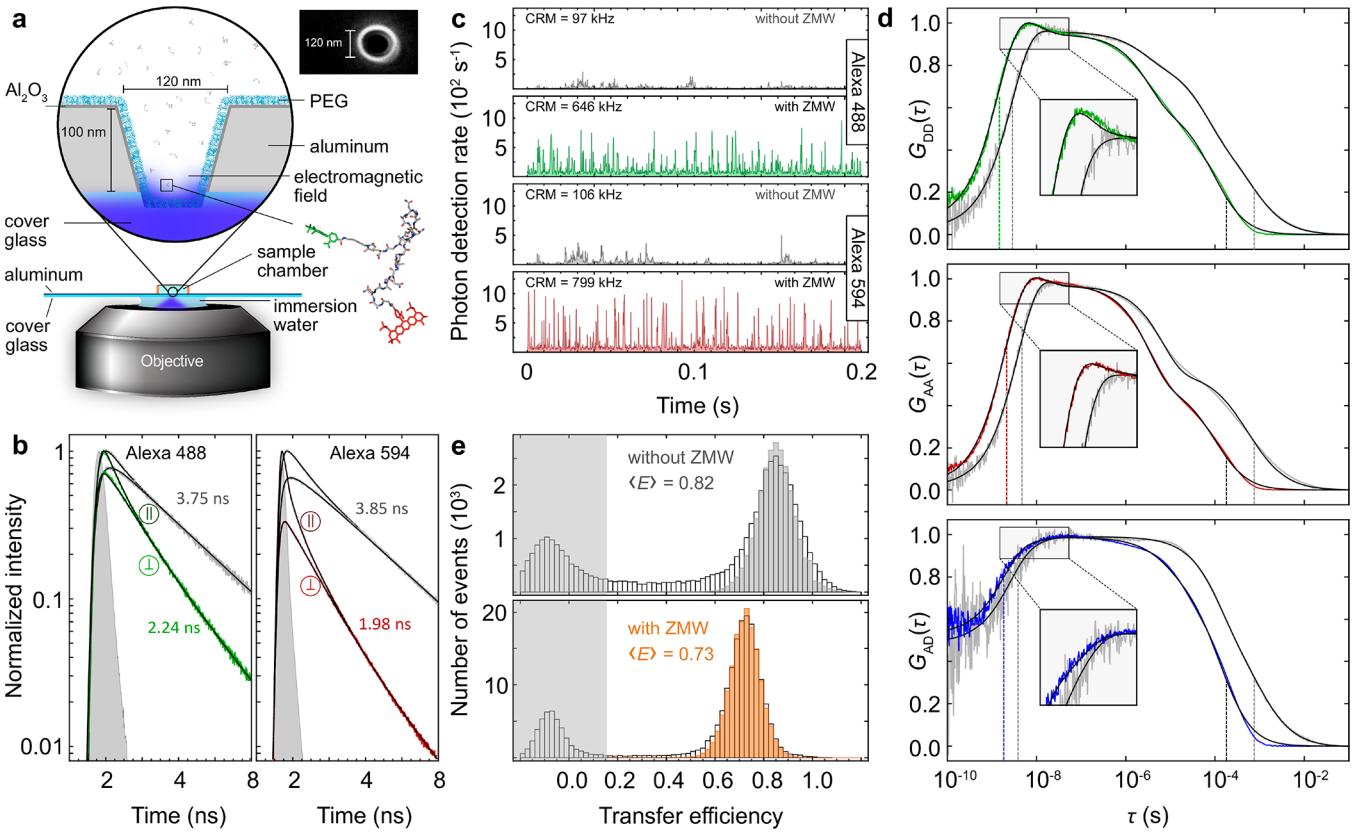

Figure 1. Enhancing nsFCS with zero-mode waveguides (ZMWs). (a) Schematic depiction of confocal measurements of the AGQ peptide labeled with Alexa 488 and 594 in a ZMW. Inset: scanning electron micrograph of a 120 nm aluminum ZMW nanoaperture (SI, Figure S1). (b) Polarization-resolved fluorescence lifetime decays of donor and acceptor measured confocally without (gray) and with ZMW (color: darker, parallel polarization; lighter, perpendicular polarization; instrument response function shaded in gray; average lifetimes from the fits (solid lines) are indicated). Donor decays are from the donor-only population, acceptor decays from the FRET population after direct acceptor excitation (see SI, Methods). (c) Time-binned (0.2 ms) fluorescence traces of donor and acceptor emission without (gray) and with ZMW (green, red), from measurements with similar average numbers of molecules in the observation volume (confocal, ~0.2; ZMW, ~0.24); average count rates per molecule (CRM, see SI, Methods) are indicated. (d) Normalized correlation functions from picoseconds to milliseconds of the labeled peptide measured without (gray, 40 h acquisition time) and with ZMW (color, 7 h acquisition time). Global fits with eq 5 (see SI, Methods) are shown as black solid lines. Insets show magnified views of the time range where distance dynamics dominate the correlations. The time scales of photon antibunching and translational diffusion with (colored, black) and without ZMW (gray) are indicated as dashed vertical lines. (e) Transfer efficiency histograms (see SI, Methods, for corrections) observed without (top) and with ZMW (bottom); black, measured; shaded, shot noise-limited photon distribution analysis.[9] All measurements shown are in 50 mM sodium phosphate, 7.4 M urea, pH 7.4.

594 attached as FRET donor and acceptor, respectively, to the termini of the short disordered peptide $G(AGQ)_6AGC$. As expected from the smaller observation volume in the 120 nm ZMWs, the translational diffusion time of this AGQ peptide is much shorter than in confocal measurements without ZMW (Figure 1d, SI, Figure S2). More importantly, however, the fluorescence lifetimes of the dyes are reduced by about 2-fold in the ZMWs (Figure 1b), and the average count rate per molecule (CRM) is enhanced by about 6−8-fold (Figure 1c, see SI, Methods). This nanophotonic enhancement of the electric field and the connected effects on the decay and transfer rates of donor and acceptor in the ZMWs are expected to cause a change in the distance dependence of the FRET efficiency.[18] The small shift in efficiency we observe (<0.1, Figure 1e) indicates only a moderate effect on the energy transfer process[17] that can be accounted for by calibration (see SI, Methods and Figure S3) and shifts sensitivity toward slightly shorter distances. Single-molecule FRET and nsFCS are thus feasible in ZMWs with this commonly used dye pair.

We use the Alexa488/594-labeled disordered AGQ peptide to assess the enhancement of nsFCS by ZMWs (Figure 2). In 7.4 M urea, where the peptide is more expanded than in the absence of denaturant (SI, Figure S3), its rapid end-to-end distance fluctuations result in a correlation time of only about twice the natural fluorescence lifetimes of the fluorophores (Figure 2a). This situation is challenging for conventional nsFCS[19] because the correlation caused by conformational dynamics overlaps with the pronounced drop of the curve at short times caused by photon antibunching (Figures 2a, SI, Figure S2). With the ZMWs, however, the reduced fluorescence lifetimes lead to a narrower photon antibunching component, and the rapid conformational dynamics can be clearly resolved in the correlation functions (Inset Figure 1d, Figure 2b, SI, Figure S2). We extract a characteristic relaxation time corresponding to conformational dynamics of 8.8 ± 0.3 ns (Figure 2b). Even in the absence of urea, where the AGQ peptide is more compact (SI, Figure S3) and the conformational dynamics are faster still, nsFCS in ZMWs can resolve the contribution from chain dynamics (Figure 2d). The observed correlation time of 4.2 ± 0.5 ns is very close to the natural fluorescence lifetimes of the dyes and thus beyond the reach of measurements without ZMWs (SI, Figure S4). Furthermore, the nanophotonic

https://doi.org/10.1021/jacs.1c09387
J. Am. Chem. Soc. 2022, 144, 52−56

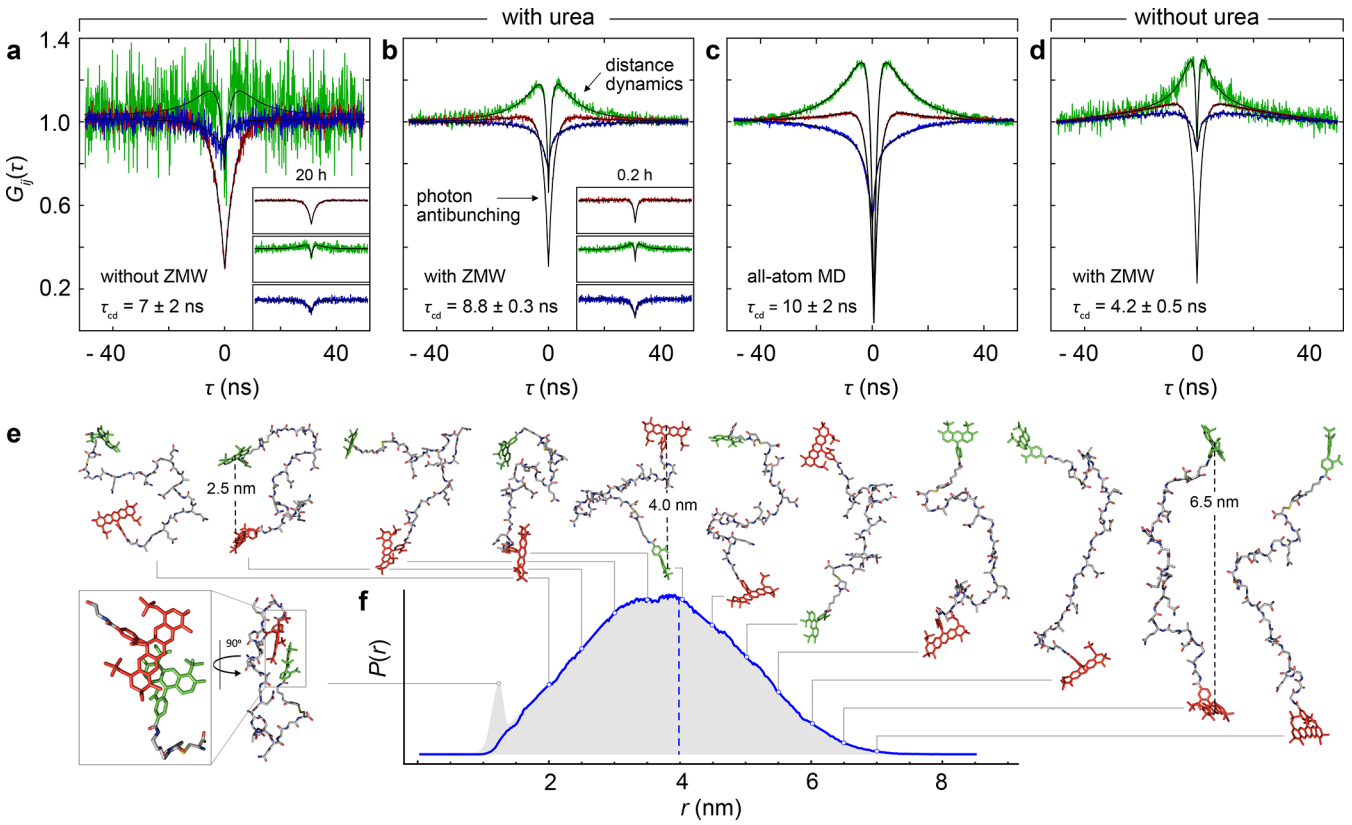

Figure 2. Probing the rapid dynamics of a disordered peptide with enhanced nsFCS. (a–c) Overlay of donor (green) and acceptor (red) fluorescence autocorrelations and donor–acceptor cross-correlations (blue) from measurements of the disordered AGQ peptide in 7.4 M urea without ZMW (a) and with ZMW (b) after 7 h of data acquisition (inset in (a) after 20 h and in (b) after 0.2 h of data acquisition) with 100 ps time binning, and comparison with fluorescence correlation curves simulated based on all-atom molecular dynamics (MD) trajectories (c) using photophysical parameters corresponding to measurements in ZMWs (black solid lines are fits with SI, eq 8, Methods, with resulting fluorescence intensity correlation times, τ_{cd}, as indicated, with uncertainties estimated from three independent measurements; see SI, Figure S7, for uncertainties of τ_{cd} in (c)). (d) nsFCS measurement with ZMW of the AGQ peptide without urea. The slight additional correlation decay visible for longer times is caused by contact quenching between donor and acceptor. (e) Representative snapshots from MD simulations of the disordered $G(AGQ)_6AGC$ peptide with explicit donor and acceptor dyes, Alexa Fluors 488 (green) and 594 (red) and various interdye distances. (f) Distance distributions, P(r), from MD simulations in 7.4 M urea (gray histogram, complete distribution; blue histogram, emissive conformations excluding dye–dye contacts; example of a configuration with stacked dyes shown to the left) with corresponding root-mean-square interdye distance, $\langle r^2 \rangle^{1/2}$ (dashed vertical line).

enhancement of the fluorescence emission rates enables a marked reduction in the data acquisition time required for a quantitative analysis of rapid chain dynamics (Figure 2b), even in mixtures of different proteins (SI, Figure S5). Instead of the typical measurement times of 10 h or more, adequate statistics can be achieved in tens of minutes (Figure 2a,b, SI, Figure S6).

The rapid distance fluctuations accessible with nsFCS measurements in ZMWs enable a direct comparison with molecular dynamics (MD) simulations to gain a detailed picture of the underlying polypeptide chain reconfiguration. We thus performed all-atom explicit-solvent MD simulations of the AGQ peptide, including explicit donor and acceptor dyes,[20,21] using a force field and water model suitable for disordered proteins, Amber99SBws/TIP4P2005s,[22] and a previously optimized parametrization of the fluorophores[23] and urea[24] (Figure 2e, and SI, Video S1). Extensive sampling of peptide conformations was ensured with 16 μs of total simulation time (SI, Figure S7). To enable a direct comparison with the measurements rather than with derived quantities, we simulated photon emission based on the MD trajectories, using the fluorescence lifetimes, excitation rates, and detector crosstalk corresponding to the experiments, including the influence of the ZMWs on the photophysics. In the simulation, the exact dye configuration is known for every simulation frame, so both the distance- and the orientation-dependence of Förster transfer can be taken into account explicitly (see SI, Methods, for details).

The resulting fluorescence correlation functions (Figure 2c) are in remarkable agreement with the experimental data (Figure 2b), suggesting a faithful representation of the peptide dynamics in the simulations. In the absence of urea, the more rapid chain relaxation is also reproduced accurately, but an additional slower component points toward a slight overestimate of dye interactions (SI, Figure S8). The agreement between the average transfer efficiencies from simulations (0.80 ± 0.01 with urea, 0.92 ± 0.01 without urea) and experiments (0.82 ± 0.03 with urea, 0.94 ± 0.03 without urea) provides an additional indication that MD simulations using current force fields with appropriately balanced protein–water interactions[22,25] can provide a realistic picture of the dynamics and conformational ensembles of disordered peptides and proteins.[26−28] Moreover, by comparing simulations of the AGQ peptide in urea with and without fluorophores, we can infer that the end-to-end distance correlation time of the unlabeled peptide is ∼30% lower than that of the labeled one (see SI, Methods). This difference is not unexpected given the size of the probes compared to this relatively small peptide (the relative contribution will be less for

https://doi.org/10.1021/jacs.1c09387
J. Am. Chem. Soc. 2022, 144, 52−56

larger IDPs), but an accurate value cannot easily be inferred from the experimental data alone.

In summary, nanophotonics-enhanced nsFCS provides new opportunities for probing rapid biomolecular dynamics. The extended range of accessible time scales in the low nanosecond regime, together with the pronounced reduction in measurement time, eliminate previous limitations of nsFCS. The method will thus enable the investigation of peptides, disordered protein regions, nucleic acids, and other biomolecules in a time range that has so far been difficult to monitor, with much higher throughput than previously possible and with less stringent demands on long-term sample stability. The method is complementary to the structural information and dynamics available from techniques such as NMR,[29,30] and we expect it to be directly transferable to other single-molecule fluorescence techniques, such as photoinduced electron transfer.[31] Finally, results from nanophotonics-enhanced nsFCS can provide stringent benchmarks for the further optimization of molecular dynamics force fields, and in synergy with the resulting simulations, they will help to obtain an increasingly detailed understanding of biomolecular dynamics over the full range of relevant time scales.

■ ASSOCIATED CONTENT

Supporting Information

The Supporting Information is available free of charge at https://pubs.acs.org/doi/10.1021/jacs.1c09387.

Materials and methods section and supplementary figures (PDF)

Video of all-atom molecular dynamics simulation of AGQ peptide in 7.4 M urea (MOV)

■ AUTHOR INFORMATION

Corresponding Authors

Benjamin Schuler − *Department of Biochemistry, University of Zurich, 8057 Zurich, Switzerland; Department of Physics, University of Zurich, 8057 Zurich, Switzerland;* orcid.org/0000-0002-5970-4251; Email: schuler@bioc.uzh.ch

Robert B. Best − *Laboratory of Chemical Physics, National Institute of Diabetes and Digestive and Kidney Diseases, National Institutes of Health, Bethesda, Maryland 20892-0520, United States;* orcid.org/0000-0002-7893-3543; Email: robert.best2@nih.gov

Jérôme Wenger − *Aix Marseille Univ, CNRS, Centrale Marseille, Institut Fresnel, 13013 Marseille, France;* orcid.org/0000-0002-2145-5341; Email: jerome.wenger@fresnel.fr

Authors

Mark F. Nüesch − *Department of Biochemistry, University of Zurich, 8057 Zurich, Switzerland*

Miloš T. Ivanović − *Department of Biochemistry, University of Zurich, 8057 Zurich, Switzerland;* orcid.org/0000-0003-3164-9411

Jean-Benoît Claude − *Aix Marseille Univ, CNRS, Centrale Marseille, Institut Fresnel, 13013 Marseille, France*

Daniel Nettels − *Department of Biochemistry, University of Zurich, 8057 Zurich, Switzerland*

Complete contact information is available at: https://pubs.acs.org/10.1021/jacs.1c09387

Notes

The authors declare no competing financial interest.

■ ACKNOWLEDGMENTS

We thank Andrea Sottini for a sample of labeled prothymosin α, and we thank Mikhail Baibakov, Satyajit Patra, Erik Holmstrom, and Hervé Rigneault for stimulating and helpful discussions. This work was supported by the Swiss National Science Foundation (B.S.), the European Research Council (ERC) under the European Union's Horizon 2020 research and innovation program (grant agreement 723241, J.W.), the Agence Nationale de la Recherche (ANR) under grant agreement ANR-17-CE09-0026-01 (J.W.), the Intramural Research Program of the NIDDK at the National Institutes of Health (R.B.B.), a grant from the Swiss National Supercomputing Centre (CSCS) under project 334, and by PRACE with access to Joliot-Curie at GENCI@CEA, France.

■ REFERENCES

(1) Selvin, P. R.; Ha, T. *Single-Molecule Techniques: A Laboratory Manual*; Cold Spring Harbor Laboratory Press: New York, 2008.

(2) Sauer, M.; Hofkens, J.; Enderlein, J. *Handbook of Fluorescence Spectroscopy and Imaging: From Single Molecules to Ensembles*. Wiley-VCH: Weinheim, 2011.

(3) Schuler, B.; Hofmann, H. Single-molecule spectroscopy of protein folding dynamics-expanding scope and timescales. *Curr. Opin. Struct. Biol.* **2013**, *23*, 36−47.

(4) Dimura, M.; Peulen, T. O.; Hanke, C. A.; Prakash, A.; Gohlke, H.; Seidel, C. A. Quantitative FRET studies and integrative modeling unravel the structure and dynamics of biomolecular systems. *Curr. Opin. Struct. Biol.* **2016**, *40*, 163−185.

(5) Juette, M. F.; Terry, D. S.; Wasserman, M. R.; Altman, R. B.; Zhou, Z.; Zhao, H.; Blanchard, S. C. Single-molecule imaging of non-equilibrium molecular ensembles on the millisecond timescale. *Nat. Methods* **2016**, *13*, 341−4.

(6) Chung, H. S.; Eaton, W. A. Protein folding transition path times from single molecule FRET. *Curr. Opin. Struct. Biol.* **2018**, *48*, 30−39.

(7) Lerner, E.; Cordes, T.; Ingargiola, A.; Alhadid, Y.; Chung, S.; Michalet, X.; Weiss, S. Toward dynamic structural biology: Two decades of single-molecule Forster resonance energy transfer. *Science* **2018**, *359*, eaan1133.

(8) Mazal, H.; Haran, G. Single-molecule FRET methods to study the dynamics of proteins at work. *Curr. Opin. Biomed. Eng.* **2019**, *12*, 8−17.

(9) Antonik, M.; Felekyan, S.; Gaiduk, A.; Seidel, C. A. Separating structural heterogeneities from stochastic variations in fluorescence resonance energy transfer distributions via photon distribution analysis. *J. Phys. Chem. B* **2006**, *110*, 6970−8.

(10) Nettels, D.; Gopich, I. V.; Hoffmann, A.; Schuler, B. Ultrafast dynamics of protein collapse from single-molecule photon statistics. *Proc. Natl. Acad. Sci. U.S.A.* **2007**, *104*, 2655−2660.

(11) Schuler, B.; Soranno, A.; Hofmann, H.; Nettels, D. Single-Molecule FRET Spectroscopy and the Polymer Physics of Unfolded and Intrinsically Disordered Proteins. *Annu. Rev. Biophys.* **2016**, *45*, 207−31.

(12) Haenni, D.; Zosel, F.; Reymond, L.; Nettels, D.; Schuler, B. Intramolecular distances and dynamics from the combined photon statistics of single-molecule FRET and photoinduced electron transfer. *J. Phys. Chem. B* **2013**, *117*, 13015−28.

(13) Levene, M. J.; Korlach, J.; Turner, S. W.; Foquet, M.; Craighead, H. G.; Webb, W. W. Zero-mode waveguides for single-molecule analysis at high concentrations. *Science* **2003**, *299*, 682−6.

(14) Zhu, P.; Craighead, H. G. Zero-Mode Waveguides for Single-Molecule Analysis. *Annu. Rev. Biophys.* **2012**, *41*, 269−293.

(15) Novotny, L.; Hecht, B. *Principles of Nano-Optics*; Cambridge University Press: Cambridge, UK.

(16) Enderlein, J. Modification of Förster Resonance Energy Transfer Efficiency at Interfaces. *Int. J. Mol. Sci.* **2012**, *13*, 15227−15240.

(17) Punj, D.; Ghenuche, P.; Moparthi, S. B.; de Torres, J.; Grigoriev, V.; Rigneault, H.; Wenger, J. Plasmonic antennas and zero- mode waveguides to enhance single molecule fluorescence detection and fluorescence correlation spectroscopy toward physiological concentrations. *Wires Nanomed Nanobi* **2014**, *6*, 268−282.
(18) Baibakov, M.; Patra, S.; Claude, J. B.; Moreau, A.; Lumeau, J.; Wenger, J. Extending Single-Molecule Forster Resonance Energy Transfer (FRET) Range beyond 10 Nanometers in Zero-Mode Waveguides. *ACS Nano* **2019**, *13*, 8469−8480.
(19) Nettels, D.; Hoffmann, A.; Schuler, B. Unfolded Protein and Peptide Dynamics Investigated with Single-Molecule FRET and Correlation Spectroscopy from Picoseconds to Seconds. *J. Phys. Chem. B* **2008**, *112*, 6137−46.
(20) Vaiana, A. C.; Neuweiler, H.; Schulz, A.; Wolfrum, J.; Sauer, M.; Smith, J. C. Fluorescence quenching of dyes by tryptophan: Interactions at atomic detail from combination of experiment and computer simulation. *J. Am. Chem. Soc.* **2003**, *125*, 14564−14572.
(21) Graen, T.; Hoefling, M.; Grubmuller, H. AMBER-DYES: Characterization of Charge Fluctuations and Force Field Parameterization of Fluorescent Dyes for Molecular Dynamics Simulations. *J. Chem. Theory Comput.* **2014**, *10*, 5505−12.
(22) Best, R. B.; Zheng, W.; Mittal, J. Balanced Protein-Water Interactions Improve Properties of Disordered Proteins and Non-Specific Protein Association. *J. Chem. Theory Comput.* **2014**, *10*, 5113−5124.
(23) Best, R. B.; Hofmann, H.; Nettels, D.; Schuler, B. Quantitative Interpretation of FRET Experiments via Molecular Simulation: Force Field and Validation. *Biophys. J.* **2015**, *108*, 2721−2731.
(24) Zheng, W. W.; Borgia, A.; Borgia, M. B.; Schuler, B.; Best, R. B. Empirical Optimization of Interactions between Proteins and Chemical Denaturants in Molecular Simulations. *J. Chem. Theory Comput.* **2015**, *11*, 5543−5553.
(25) Robustelli, P.; Piana, S.; Shaw, D. E. Developing a molecular dynamics force field for both folded and disordered protein states. *Proc. Natl. Acad. Sci. U.S.A.* **2018**, *115*, E4758−E4766.
(26) Shrestha, U. R.; Juneja, P.; Zhang, Q.; Gurumoorthy, V.; Borreguero, J. M.; Urban, V.; Cheng, X.; Pingali, S. V.; Smith, J. C.; O'Neill, H. M.; Petridis, L. Generation of the configurational ensemble of an intrinsically disordered protein from unbiased molecular dynamics simulation. *Proc. Natl. Acad. Sci. U.S.A.* **2019**, *116*, 20446−20452.
(27) Graen, T.; Klement, R.; Grupi, A.; Haas, E.; Grubmuller, H. Transient Secondary and Tertiary Structure Formation Kinetics in the Intrinsically Disordered State of alpha-Synuclein from Atomistic Simulations. *ChemPhysChem* **2018**, *19*, 2507−2511.
(28) Zerze, G. H.; Mittal, J.; Best, R. B. Diffusive Dynamics of Contact Formation in Disordered Polypeptides. *Phys. Rev. Lett.* **2016**, *116*, 068102.
(29) Rezaei-Ghaleh, N.; Parigi, G.; Soranno, A.; Holla, A.; Becker, S.; Schuler, B.; Luchinat, C.; Zweckstetter, M. Local and Global Dynamics in Intrinsically Disordered Synuclein. *Angew. Chem., Int. Ed.* **2018**, *57*, 15262−15266.
(30) Milles, S.; Salvi, N.; Blackledge, M.; Jensen, M. R. Characterization of intrinsically disordered proteins and their dynamic complexes: From in vitro to cell-like environments. *Prog. Nucl. Magn. Reson. Spectrosc.* **2018**, *109*, 79−100.
(31) Sauer, M.; Neuweiler, H. PET-FCS: probing rapid structural fluctuations of proteins and nucleic acids by single-molecule fluorescence quenching. *Methods Mol. Biol.* **2014**, *1076*, 597−615.

https://doi.org/10.1021/jacs.1c09387
J. Am. Chem. Soc. 2022, 144, 52−56

Supporting Information

Single-molecule detection of ultrafast biomolecular dynamics with nanophotonics

Mark F. Nüesch, Miloš T. Ivanović, Jean-Benoît Claude, Daniel Nettels, Robert B. Best*, Jérôme Wenger*, Benjamin Schuler*

Materials and Methods

ZMW fabrication and surface passivation. Zero-mode waveguide (ZMW) apertures (Figure S1) with a diameter of 120 nm were milled into 100 nm thick aluminum layer deposited on a glass coverslip with a focused ion beam (FEI Strata Dual Beam 235) as previously described[1]. Prior to the experiments, the ZMWs were rinsed with double-distilled water and absolute ethanol (≥ 99.7%) to remove dust. The ZMWs were further cleaned and activated by a 5-min air plasma exposure (FEMTO, Diener, driven at 75%), immediately followed by incubation in 1 mg/mL silane-modified polyethylene glycol of molecular weight 1000 Da (PEG 1000 Lysane Bioc. Inc. USA) dissolved in absolute ethanol containing 1% acetic acid for 12h at room temperature in N_2 atmosphere. After incubation, the nanoapertures were washed with ethanol containing 1% Tween 20 to remove unadsorbed PEG-silane. After a final rinse with absolute ethanol and double distilled water, the structures were dried in a flow of air. Surface-passivated ZMWs were stored dry at room temperature. The agreement of the transfer efficiencies and relaxation times with and without ZMWs indicates the absence of pronounced perturbations owing to surface interactions in the nanoapertures. A quantitative assessment of the efficiency of surface passivation by PEG 1000 is shown in Figure S9. The diameter of 120 nm for the ZMWs was chosen based on a screen of the influence of ZMWs with different diameters (80 nm – 250 nm) on the molecular brightness enhancement and fluorescence lifetime reduction of the Alexa Fluors 488 and 594, where an optimum was observed at around 120 nm.[2-3] Individual devices could typically be used for several days in contact with sample solution until noticeable corrosion of the aluminum layer was detected, which reduces the performance of the ZMWs.

Protein preparation. The disordered AGQ peptide $G(AGQ)_6AGC$ was purchased from GL Biochem (Shanghai, China), purified, and labeled with Alexa Fluors 488 and 594 as previously described[4].

Single-molecule spectroscopy and data reduction. Single-molecule fluorescence experiments with and without ZMWs were performed on a four-channel MicroTime 200 confocal instrument (PicoQuant) equipped with an Olympus UplanApo 60x/1.20 W objective. Alexa488 was excited with a diode laser (LDH-D-C-485, PicoQuant) at an average power of 100 µW (measured at the back aperture of the objective). The laser was operated in continuous-wave mode for nsFCS experiments and in pulsed mode with interleaved acceptor excitation for fluorescence lifetime measurements[5]. The wavelength range used for acceptor excitation was selected with two band pass filters (z582/15 and

z580/23, Chroma) from the emission of a supercontinuum laser (EXW-12 SuperK Extreme, NKT Photonics) driven at 20 MHz (45 µW average laser power after the band pass filters), which also triggered interleaved pulses from the 488-nm diode laser. Sample fluorescence was collected by the microscope objective, separated from backscattered light with a triple band pass filter (r405/488/594, Chroma) and focused on a 100-µm pinhole. After the pinhole, fluorescence emission was separated into two channels, either with a polarizing beam splitter for fluorescence lifetime measurements, or with a 50/50 beam splitter for nsFCS measurements to avoid the effects of detector deadtimes and afterpulsing on the correlation functions[6]. Finally, the fluorescence photons were separated by wavelength into four channels by dichroic mirrors (585DCXR, Chroma), additionally filtered by bandpass filters (ET525/50M and HQ650/100, Chroma), and focused onto one of four single-photon avalanche detectors (SPCM-AQRH-14-TR, Excelitas). The arrival time of every detected photon was recorded with a HydraHarp 400 counting module (PicoQuant, Berlin, Germany).

Single-molecule photon trajectories of freely diffusing FRET labeled molecules with and without ZMWs (concentrations of labeled molecules with ZMWs 100-310 nM, without 100-500 pM) were inspected for the absence of slow intensity variations, especially for measurements in ZMWs, which are sensitive to even slight drifts of the microscope stage. Selected trajectories were binned (0.2-ms bins with ZMWs, 1-ms bins without ZMW), and bursts of photons were identified with a threshold of 50 photons per time bin and contiguous identified bins combined into one burst. Corrected transfer efficiencies, E, and corrected fluorescence stoichiometry ratios, S, were then calculated according to[7-8]

$$E = \frac{n_{\mathrm{DA}} - \beta\, n_{\mathrm{DD}} - d\, n_{\mathrm{AA}}}{n_{\mathrm{DA}} - \beta\, n_{\mathrm{DD}} - d\, n_{\mathrm{AA}} + \gamma\, n_{\mathrm{DD}}} \qquad (1)$$

and

$$S = \frac{n_{\mathrm{DA}} - \beta\, n_{\mathrm{DD}} - d\, n_{\mathrm{AA}} + \gamma\, n_{\mathrm{DD}}}{n_{\mathrm{DA}} - \beta\, n_{\mathrm{DD}} - d\, n_{\mathrm{AA}} + \gamma\, n_{\mathrm{DD}} + \gamma_{PIE}\, n_{\mathrm{AA}}}, \qquad (2)$$

where n_{DA} and n_{DD} are the uncorrected acceptor and donor detector counts after donor excitation, and n_{AA} the uncorrected acceptor detector counts after direct acceptor excitation. β is the correction factor for spectral crosstalk, d for acceptor direct excitation, γ for differences in quantum yields and detection efficiencies, and γ_{PIE} for differences in excitation rates. The corrections for spectral crosstalk and direct excitation were determined as previously described from the donor-only and acceptor-only populations of the measurements[7-8]. For determining γ and γ_{PIE}, at least two FRET populations are needed[7-8]. Therefore, we measured a second sample (prothymosin α, ProTα, labeled with Alexa Fluors 488 and 594 at positions E56C and D110C[9-10]) with a mean transfer efficiency much lower than that of the AGQ peptide. As shown previously, these correction parameters can be influenced by the presence of a ZMW[3, 11-12]. Hence we determined corrections both with and without ZMWs. Representative 2D histograms of FRET efficiency vs. stoichiometry ratio are shown in Figure S3. The *E* values from all identified bursts of each measurement were represented in a transfer efficiency histogram, and the subpopulation corresponding to the FRET-labeled species was fitted with a Gaussian peak function (see Figure S3) or analyzed by photon distribution analysis (PDA) taking into account the experimentally observed burst size distribution[13-15] (Figure 1e, Figure S5). Comparison with PDA indicates that the widths of the peaks in the transfer efficiency histograms are close to the expected shot-noise limit, both for measurements without and with ZMWs (Figure 1e, Figure S5). The slightly more pronounced broadening beyond shot noise observed for nsFCS measurements performed

without ZMW (Figure 1e) is most likely caused by the relatively high concentration of labeled sample that is typically used in such measurements (~500 pM) to optimize the signal-to-noise ratio for nsFCS. Under these conditions, a separation of subpopulations is still possible, but some two-molecule events contribute to the signal. This effect also explains the larger number of bursts with an apparent transfer efficiency between the donor-only and the FRET-active population (Figure 1e).

The differences between the corrected transfer efficiencies with and without ZMWs suggest a change in the distance dependence of the FRET efficiency, $E(r)$, as observed previously[3, 11-12]. To estimate the required correction, we described the distance distributions, $P(r)$, of ProTα and the AGQ peptide with the SAWv polymer model[16] using the corrected mean transfer efficiencies from the measurements without ZMW according to[17]

$$\langle E \rangle = \int_0^\infty E(r)P(r)dr, \tag{3}$$

where $E(r) = R_0^6/(R_0^6 + r^6)$ and R_0 = 5.4 nm.[18] In the presence of urea, R_0 was corrected for the corresponding change in refractive index[19]. The resulting distance distributions were used to globally fit the distance dependence of the transfer efficiencies measured in the ZMW with Eq. 3, using R_0 as a shared fit parameter. The resulting dependence is empirically well described by $E(r) = 1/(1 + (r/R_0)^6)$ with R_0 = 4.71 nm without urea and 4.56 nm in 7.4 M urea (Extended Data Table 1).

Fluorescence correlation spectroscopy (FCS). Measurements were performed on freely diffusing Alexa 488/595-labeled AGQ peptides in two different solution conditions, both with and without ZMWs. One set of measurements was performed in 50 mM sodium phosphate buffer pH 7.4 in the presence of 7.4 M urea, and a second set in 50 mM sodium phosphate buffer pH 7.4 in the absence of urea (referred to as "with urea" and "without urea", respectively, in the text). Additionally, we included 140 mM β-mercaptoethanol as a photoprotectant[20] and 0.01% Tween 20 (Pierce) to minimize surface adhesion[21]. The concentration of labeled AGQ peptide was 500 pM and 310 nM for measurements without and with ZMWs, respectively. The sample chamber used for measurements without ZMWs was a plastic well (μ-slide, Ibidi GmbH) with a volume of 50 μL; a perfusion chamber with a volume of 40 μL was used for measurements with ZMWs (CoverWell, GRACE BIO-LABS). To prevent evaporation, sample chambers were sealed with adhesive tape (Scotch). Sample stability was ensured by monitoring the observed fluorescence intensity during the measurements and by comparing correlations obtained from different segments of the recorded data (see Figure S9c).

The correlation between two time-dependent intensity signals $I_i(t)$ and $I_j(t)$ measured on two detectors i and j is defined as

$$G_{ij}(\tau) = \frac{\langle I_i(t)I_j(t+\tau)\rangle}{\langle I_i(t)\rangle\langle I_j(t)\rangle} - 1, \tag{4}$$

where the pointed brackets indicate averaging over t. In our experiments, we use two acceptor channels and two donor channels, resulting in the autocorrelations $G_{AA}(\tau)$ and $G_{DD}(\tau)$, and cross-correlations $G_{AD}(\tau)$ and $G_{DA}(\tau)$. By correlating detector pairs, and not the signal from a detector with itself, contributions to the correlations from dead times and after-pulsing of the detectors are eliminated[6, 22]. Full FCS curves as shown with logarithmically spaced lag times ranging from nanoseconds to seconds (Figure 1d, S2) were fitted with[4, 23]

$$G_{ij}(\tau) = a_{ij}\,\frac{(1 - c_{ab}^{ij}\,e^{-|\tau|/\tau_{ab}^{ij}})(1 + c_{cd}^{ij}\,e^{-|\tau|/\tau_{cd}})(1 + c_{Q}^{ij}\,e^{-|\tau|/\tau_{Q}})(1 + c_{T}^{ij}\,e^{-|\tau|/\tau_{T}^{ij}})}{\left(1 + \frac{|\tau|}{\tau_D}\right)\left(1 + \frac{|\tau|}{s^2\,\tau_D}\right)^{1/2}}. \quad (5)$$

The four terms in the numerator with amplitudes c_{ab}, c_{cd}, c_Q, c_T, and timescales $\tau_{ab}, \tau_{cd}, \tau_Q, \tau_T$ describe photon antibunching, chain dynamics, quenching, and triplet blinking, respectively. τ_D is the translational diffusion time of the labeled molecules through the confocal volume; a point spread function (PSF) of 3-dimensional Gaussian shape is assumed, with a ratio of axial over lateral radii of $s = \omega_z/\omega_{xy}$ (s = 5.3 without and s = 1.0 with ZMW; note that this PSF is not expected to be a good approximation for the confocal volume in the ZMWs but has been commonly used owing to a lack of suitable alternatives[1, 24]). Parameters without indices *ij* are treated as shared parameters in the global fits of the auto- and crosscorrelation functions.

The amplitude a_{ii} of the autocorrelations can be written as:

$$a_{ii} = \frac{1}{N_i}\left(1 - \frac{\langle B_i \rangle}{\langle I_i \rangle}\right)^2, \quad (6)$$

where N_i is the average number of labeled molecules present in the confocal volume, and $\langle I_i \rangle$ and $\langle B_i \rangle$ are the time-averaged total intensity and the background intensity on summed over both donor detectors ($i = D$) or both acceptor detectors ($i = A$), respectively. (Note that we assume here approximately equal signals on both detector pairs.) From these quantities, we can calculate the average count rate per molecule[25], $CRM_i = (\langle I_i \rangle - \langle B_i \rangle)/N_i$. We obtained $\langle B_D \rangle$ and $\langle B_A \rangle$ from fitting photon counting histograms[26] (PCH) with a time binning of 3 µs.

The signal-to-noise ratio (S/N) in FCS in the regime relevant for monitoring fast dynamics can be expressed as[23, 25]

$$\left(\frac{S}{N}\right)_i \propto \frac{CRM_i\sqrt{\Delta\tau\; t_{acq}}}{\left(1 + \frac{1}{N_i}\right)^2}, \quad (7)$$

where $\Delta\tau$ is the lag time bin width, t_{acq} is the data acquisition time. Using Eq. 7, we found an (8 ± 2)-fold *S/N* improvement in the presence of the ZMW for both donor and acceptor, where the uncertainty was estimated from the differences in background values and count rates per molecule obtained from analyzing photon counting histograms[26] or FCS curves[25].

To study the fast dynamics in more detail, subpopulation-specific donor and acceptor fluorescence auto- and crosscorrelation curves were computed and analyzed over a linear range of lag times from $\tau = -50$ to +50 ns, as previously decribed[27-28]. For this analysis, we used only photons of bursts with *E* in the range of ± 0.2 of the mean transfer efficiency of the population of molecules double-labeled with active donor and acceptor fluorophores, which reduces the contribution of donor-only and acceptor-only signal to the correlation. To aid their direct comparison, correlation curves were normalized to unity at $\tau = 50$ ns. After normalization and in the limit of $|\tau| \ll \tau_T^{ij}$ and $|\tau| \ll \tau_D^{ij}$, Eq. 5 reduces to:

$$G_{ij}(\tau) = b_{ij}\left(1 - c_{ab}\,e^{-\frac{|\tau|}{\tau_{ab}}}\right)\left(1 + c_{cd}\,e^{-\frac{|\tau|}{\tau_{cd}}}\right)\left(1 + c_{Q}^{ij}\,e^{-\frac{|\tau|}{\tau_{Q}}}\right), \quad (8)$$

where b_{ij} is the normalization constant. For the analysis of the data without urea, the quenching timescale was fixed to the value obtained by the analysis of the complete correlation curves (τ_Q =220 ns, Figure S2). In the presence of urea, the correlation curves showed no signs of quenching, so the third term on the right-hand side of Eq. 2 could be set to unity. Fits to the data acquired without ZMWs are shown in Figure S4, and data acquired in ZMWs are shown in Figure 2. *S*/*N* for these correlations was calculated with $\Delta\tau$ = 100 ps (Eq. 7).

To quantitatively asses the efficiency of surface passivation, we compared FCS curves in non-passivated ZMWs with measurements acquired in PEG 1000-passivated ZMWs (Figure S9). To quantify the contribution of a slow-diffusion component indicating persistent surface interactions, the correlation curve was fitted with a two-species diffusion model[1] (the triplet contribution was negligible in the donor-acceptor crosscorrelation employed for analysis):

$$G(\tau) = A1\left(1+\frac{|\tau|}{\tau_{D1}}\right)^{-1}\left(1+\frac{|\tau|}{s^2\,\tau_{D1}}\right)^{-1/2} + A2\left(1+\frac{|\tau|}{\tau_{D2}}\right)^{-1}\left(1+\frac{|\tau|}{s^2\,\tau_{D2}}\right)^{-1/2}, \qquad (9)$$

where $A1$ and $A2$ are the fractions of the diffusive species with diffusion times τ_{D1} and τ_{D2} through the observation volume.

Fluorescence lifetime measurements and analysis. Data for fluorescence lifetime measurements with and without ZMWs were acquired in 50 mM sodium phosphate buffer pH 7.4 in the presence and urea absence of urea with the same additives as mentioned above and fluorescently labeled peptide at concentrations of 100 pM and 100 nM, respectively. The perpendicular, I_s, and parallel, I_p, intensity decays of the polarization-resolved time-correlated single-photon counting (TCSPC) histograms were analyzed globally using a convolution of the instrument response function (IRF) and a model decay function (Eq. 10):

$$I_s(t) = \left(1-(1-3L_2)\,r_0\,e^{\left(\frac{-t}{\tau_r}\right)}\right)\sum_{i=1}^{n}\alpha_i e^{\left(\frac{-t}{\tau_i}\right)} + c_s$$

$$I_p(t) = \left(1+\,(2-3L_1)\,r_0\,e^{\left(\frac{-t}{\tau_r}\right)}\right)G\sum_{i=1}^{n}\alpha_i e^{\left(\frac{-t}{\tau_i}\right)} + c_p\,, \qquad (10)$$

where r_0 = 0.38 is the limiting anisotropy of the dyes[29]; L_1 = 0.268 and L_2 = 0.189 are correction factors accounting for the optical path and the high-numerical-aperture objective in the confocal setup[30]; *G* accounts for the different detection efficiencies of vertically and horizontally polarized light; and c_p and c_s are background values of the vertically and horizontally polarized emission, respectively. The rotational correlation times of the fluorophores, τ_r, for donor and acceptor dye, respectively, were each globally fitted using the TCSPC histograms measured with and without ZMWs. The summation terms in Eq. 9 describe the fluorescence lifetime decays, with α_i and τ_i representing the amplitudes and relaxation times, respectively, of the individual lifetime decay components. To exclude the influence of the FRET process on the fluorescence lifetime of the donor, we analyzed TCSPC histograms from the donor-only subpopulation originating from molecules without active acceptor. The fluorescence lifetime decay of the acceptor was obtained from the FRET population after direct excitation of the acceptor. For the TCSPC histograms measured without ZMWs, single-exponential lifetime decays were found to be sufficient, whereas triple-exponential fits were used in the presence of ZMWs. In the case of multiexponential fits, the intensity-weighted average lifetime was used:

$$\langle \tau \rangle = \frac{\sum_{i=1}^{n} a_i \tau_i^2}{\sum_{i=1}^{n} a_i \tau_i}. \quad (11)$$

In the ZMWs, a very fast decay component (10 ps) was observed in the acceptor emission channel with polarization parallel to the acceptor excitation laser due to reflection of the excitation light from the metal film[1]. This component was included in the fit but excluded from the components contributing to the fluorescence lifetime.

Molecular dynamics simulations. The initial all-atom configuration of the AGQ peptide with explicit Alexa 488 and Alexa 594 dyes was generated using CHARMM[31] as described previously[32]. The structure was placed in a 7.5-nm truncated octahedral box, and the energy of the system was minimized with the steepest-descent algorithm. 1450 urea molecules were inserted into the simulation box (urea concentration: ~7.4 M) and the system was energy-minimized. Subsequently, the simulation box was filled with TIP4P2005s water[33]. 28 sodium and 23 chloride ions were added to the simulation box (ionic strength: ~128 mM) to match the ionic strength of the buffer used in the experiment and to keep the system electrostatically neutral. Subsequently, the system was again energy-minimized. The energy-minimized structure was equilibrated in a 10-ps simulation run with the Berendsen barostat[34] (τ = 5 ps), followed by a 100-ns run with the Parrinello-Rahman barostat[35] (τ = 5 ps). The final structure from this equilibration was used as a starting structure for 15 independent production simulations. All simulations were performed using GROMACS[36] 2020.3. Protein interactions were modeled using Amber99SBws[33], with protein-dye and dye-dye interaction parameters[32] as well as protein-urea, urea-urea, and water-urea parameters[37] as described previously. The temperature was kept constant at 295.15 K using velocity rescaling[38] (τ = 1 ps), and the pressure was kept at 1 bar. Long-range electrostatic interactions were modeled using the particle-mesh Ewald method[39]. Dispersion interactions and short-range repulsion were described by a Lennard-Jones potential with a cutoff at 1 nm. H-bond lengths were constrained using the LINCS algorithm[40].

The length of 15 production simulations was between 0.96 μs and 1.21 μs, resulting in a total simulation time of 15.99 μs, with a timestep of 2 fs. The first 20 ns of each simulation were excluded from the analysis to remove the initial structure bias, leaving a total of 15.69 μs of simulation time for the analysis. System coordinates were saved every Δ=5 ps. Simulations without urea were performed almost identically to the simulations with urea, but in a slightly smaller simulation box (7.0 nm truncated octahedron) containing 25 sodium and 20 chloride ions (ionic strength: ~128 mM). 17 independent production simulations were performed with a total length of 16.14 μs. The first 20 ns of each simulation were excluded from the analysis, leaving the total of 15.8 μs. Convergence of both sets of simulations was tested by analyzing the distance distribution of different parts of the total simulations as shown in Figure S7. To assess the influence of the fluorophores on peptide dynamics, simulations of unlabeled AGQ peptide with acetylated N-terminus in urea were performed analogously with a total simulation time of 10.2 μs. End-to-end distance relaxation times of the peptide with and without dyes were quantified based on single-exponential fits to the time correlations of the C^{α}-C^{α} distance between the terminal Cys and Gly residues, resulting in 10 ± 2 ns and 7 ± 2 ns, respectively.

Transfer efficiencies and nsFCS from MD simulations. Transfer efficiencies were calculated from the molecular dynamics simulations performed with and without urea and with and without ZMW using the corresponding $E(r)$ and the experimentally determined photophysical parameters. In a first step, the survival probability of the donor excited state with a fluctuating transfer rate, averaged over all possible time origins t_0 along the simulation trajectory was calculated[32, 41]:

$$p_{D^*}(t) = \langle \exp\left(-\int_{t_0}^{t_0+t} \left(k_D + k_F(t')\right)dt'\right)\rangle_{t_0}, \quad (12)$$

where

$$k_F(t) = k_D \frac{\kappa^2(t)}{2/3}\left(\frac{R_0}{r(t)}\right)^6. \quad (13)$$

κ^2 denotes the orientational factor for a specific relative orientation of donor and acceptor dye, and r the inter-dye distance. R_0 is the Förster radius for $\kappa^2 = 2/3$ and was chosen according to the presence or absence of urea and ZMW (Extended Data Table 2). κ^2 and r were calculated from the MD trajectory using simulation snapshots spaced by 5 ps. k_D was obtained from lifetime measurements of the donor-only population with and without ZMW (Figure 1b, Table 1). The dyes were treated as non-emissive when the distance between any two atoms of donor and acceptor was less than 0.4 nm, corresponding to van-der-Waals contact.[42-43] In addition, a very small fraction of frames (< 0.06 %) in which the peptide interacted with itself across the periodic image was omitted from the analysis. The average FRET efficiency, $\langle E \rangle$, from the simulations was calculated by integration over $p_{D^*}(t)$: [32, 41]

$$\langle E \rangle = 1 - k_D \int_0^{t_{max}} p_{D^*}(t)dt, \quad (14)$$

where t_{max} = 20 ns represents the time after excitation by which $p_{D^*}(t)$ is essentially zero[32]. A comparison of calculated and measured transfer efficiencies with experimentally determined parameters used for the calculation is shown in Extended Data Table 1.

Fluorescence intensity correlations were obtained from all-atom simulations by simulating photon emission based on the individual MD trajectories following the approach previously described[44]. In brief, a rate matrix (**K**) describes the transitions between the four states of the underlying photophysical model of the FRET-labeled system[45-47]: donor and acceptor in the electronic ground state (DA), donor excited/acceptor in the ground state (D*A), donor in the ground state/acceptor excited (DA*) and both donor and acceptor excited (D*A*). For low excitation rates, the population of D*A* is negligible[47], but in view of the high excitation rates in ZMWs[48-49], we explicitly accounted for D*A*, which can be populated via DA*→D*A* and D*A→D*A* with the rate coefficients k_{exD} and k_{exA}. D*A* is depopulated by singlet-singlet annihilation (SSA) with a rate coefficient k_{SSA}(t) similar in magnitude to that of the regular FRET process[47]. The evolution of the populations of these four states (DA, D*A, DA*, D*A*) with time, **p**(t), is given by the rate equation d**p**/dt = **K**(t) **p**(t), with the time-dependent rate matrix[47]

$$\mathbf{K}(t) = \begin{pmatrix} -k_{exD} - k_{exA} & k_D & k_A & 0 \\ k_{exD} & -k_D - k_{exA} - k_F(t) & 0 & k_A \\ k_{exA} & k_F(t) & -k_A - k_{exD} & k_D + k_F(t)\,\omega \\ 0 & k_{exA} & k_{exD} & -k_D - k_A - k_F(t)\,\omega \end{pmatrix}, \quad (15)$$

where $\omega = k_{SSA}/k_F(r)$= 0.95; k_{exD} = 0.02/ns · ξ and $k_{exA} = d\,k_{exD}$ are the excitation rates[6]; $k_D = 1/\langle\tau_D\rangle$ and $k_A = 1/\langle\tau_A\rangle$ are the fluorescence decay rate coefficients for the acceptor and the donor in the absence of energy transfer, respectively. The acceptor direct excitation coefficient, d, and the mean fluorescence lifetimes of the donor, $\langle\tau_D\rangle$, and the acceptor, $\langle\tau_A\rangle$, are experimentally determined values, and $k_F(t)$ is given by Eq. 13, with $\kappa^2(t)$ and $r(t)$ obtained from the MD simulations using a snapshot every Δ=5 ps. A gain in excitation rate of ξ = 3.7 was estimated from[49]

$$\xi = \sqrt{\frac{k_D^{ZMW}}{k_D^{Conf}} \frac{CRM^{ZMW}}{CRM^{Conf}}}. \quad (16)$$

Starting from the ground state (DA) at time t = 0, we repeatedly propagate through all snapshots of the MD simulation and emulate random transitions according to transition probabilities calculated using $\mathbf{I} + \mathbf{K}(t)\Delta$, where $\mathbf{I}$ is the identity matrix. For radiative transitions, photons are emitted. D*A→ DA and D*A*→ DA* transitions are accompanied by the emission of a donor photon; and DA*→ DA by an acceptor photon. Upon the transition D*A*→ D*A, an acceptor photon is emitted with probability $\frac{k_A}{k_A+k_F(t)\omega}$ because SSA is nonradiative. The quantum yields of the dyes have no effect on the resulting FCS curves and are set to one for simplicity. The dyes were treated as non-emissive when the distance between any two atoms of donor and acceptor was less than 0.4 nm, corresponding to van-der-Waals contact.[42-43] 8.8 % of the donor photons were randomly recorded as acceptor photons to mimic the influence of cross-talk between the detection channels. The propagation trough the MD simulation trajectory was repeated ~15,000 times to reach a total number of simulated photons similar to the number of measured photons used for calculating the correlations from the experiment. Fluorescence intensity correlations from simulations with and without urea were computed from the individual simulation runs; the resulting individual correlation curves thus obtained were weighted according the trajectory length, averaged, and fitted with Eq. 8 (Figures 2, S7, S8), in the same way as the experimental correlation curves.

Figure S1. Scanning electron microscopy micrograph of zero mode waveguides.

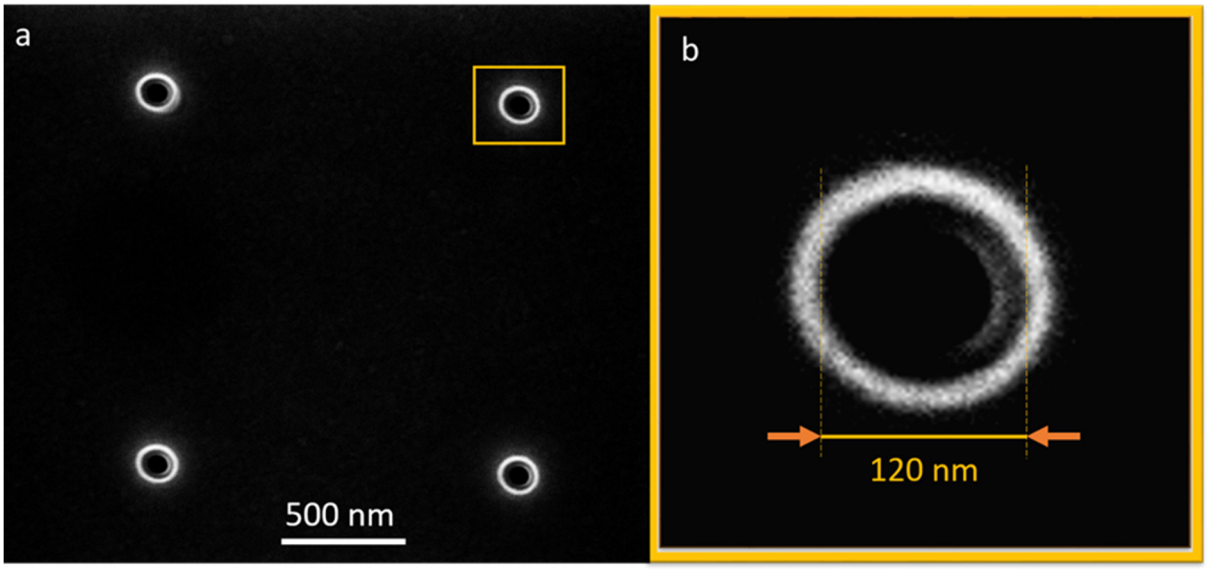

Scanning electron microscopy micrograph of zero mode waveguides (a) with zoom of a nanoaperture (b) in top view, with diameter indicated. The structures were produced by focused ion-beam milling in a 100-nm thick aluminum layer deposited on a glass cover slide.

Figure S2. Comparison of complete correlation curves of the labeled AGQ peptide with and without urea from picoseconds to milliseconds.

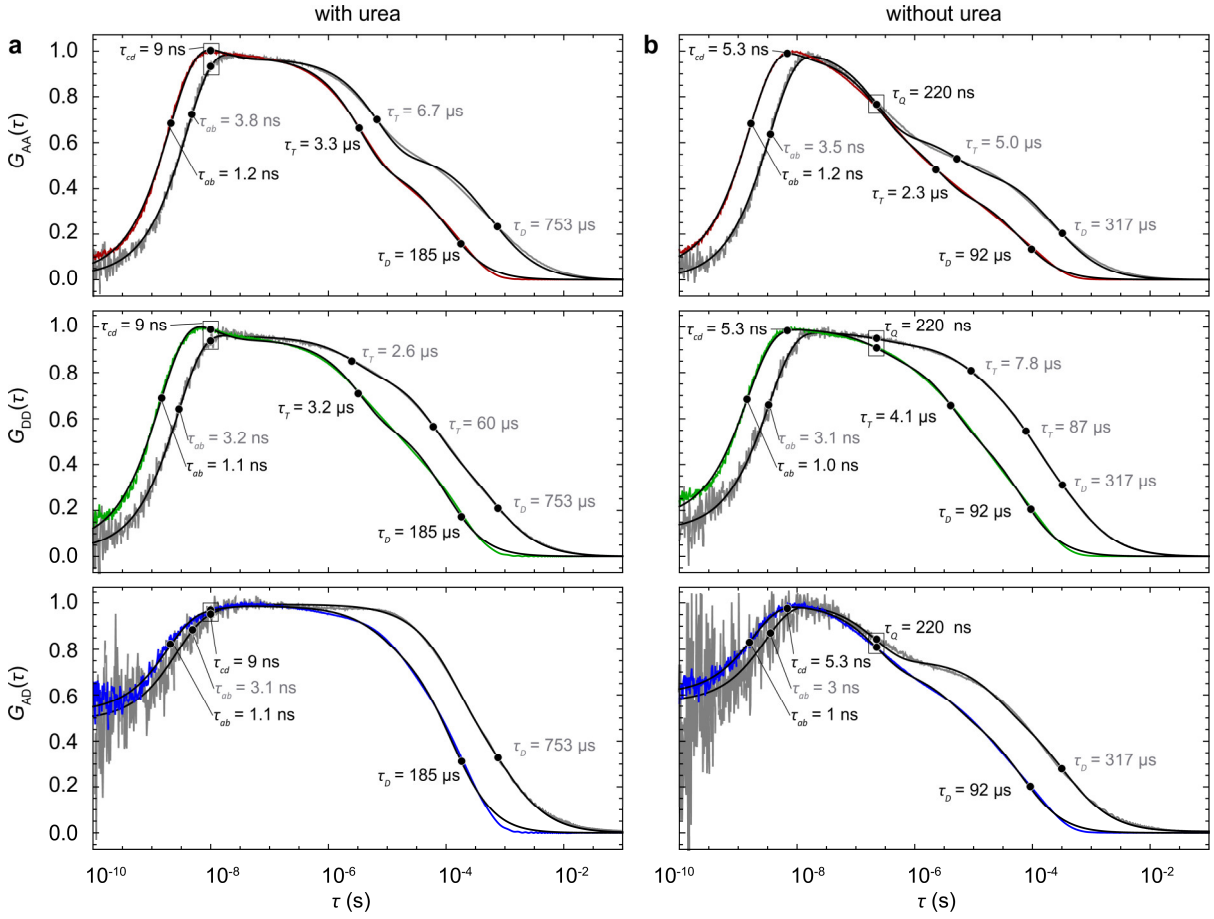

Donor and acceptor autocorrelations (with ZMW: green, red; without ZMW: gray) and donor-acceptor crosscorrelations (with ZMW: blue; without ZMW: gray) for the AGQ peptide measured with 7.4 M urea (a) and without urea (b). The fits with Eq. 5 (global fit, see Methods) are shown as black solid lines. Timescales for translational diffusion ($\boldsymbol{\tau_D}$), triplet blinking ($\boldsymbol{\tau_T}$), dye-dye quenching ($\boldsymbol{\tau_Q}$), conformational dynamics ($\boldsymbol{\tau_{cd}}$), and photon antibunching ($\boldsymbol{\tau_{ab}}$) are indicated in the figure. The shape factor $\boldsymbol{s}$ = ω_z/ω_{xy} was treated as a shared parameter for the measurements with ZMW (s = 1.0) and without ZMW (s = 5.3), respectively. Diffusion times were obtained by globally analyzing the autocorrelations and the crosscorrelation from each measurement. $\boldsymbol{\tau_Q}$ (b) and $\boldsymbol{\tau_{cd}}$ were treated as a shared parameter for the individual measurements. Note that in measurements without urea and without ZMW, no conformational dynamics could be detected due to the pronounced overlap with the antibunching timescale.

Figure S3. Comparison of transfer efficiencies measured with and without ZMWs and calibration for quantitative FRET.

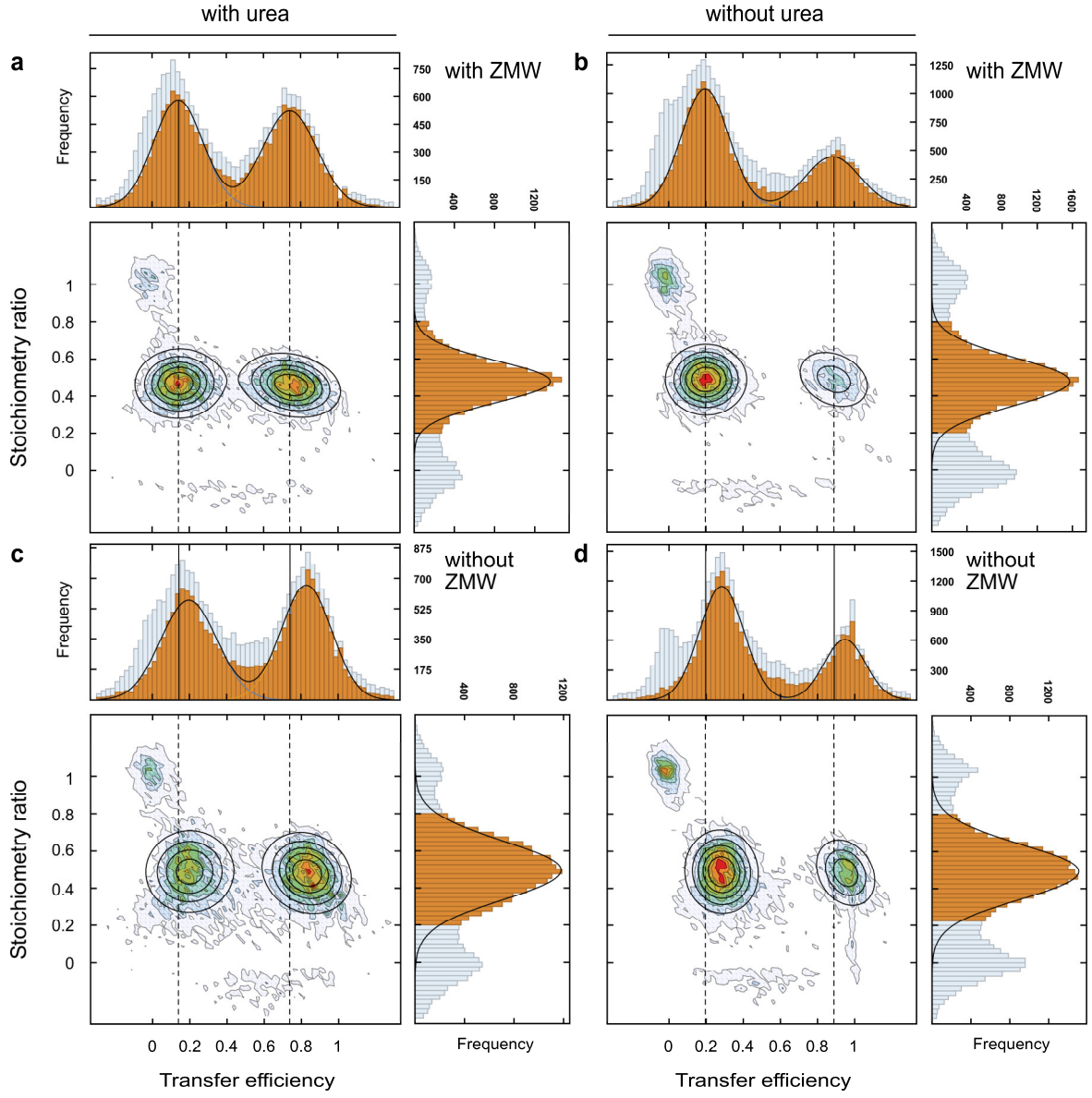

2D histograms of stoichiometry ratio (*S*) versus transfer efficiency (*E*) with ZMW (a,b) or without (c,d), recorded either with (a,c) or without urea (b,d) using a mixture of the AGQ peptide and ProTα[9] labeled with Alexa 488 and 594 (without ZMW: 50 pM each; with ZMW: 50 nM each). The FRET population at low *E* corresponds to ProTα, the population at high *E* to the AGQ peptide. The black ellipses indicate 2D Gaussian fits. Gray histograms show all observed fluorescently labeled molecules, including donor-only- ($S \approx 1$) and acceptor-only-labeled molecules ($S \approx 0$) as well as acceptor/donor-labeled molecules ($S \approx 0.5$). Orange histograms show *E* (top) and *S* (side) of the FRET-active populations identified with a threshold of 50 photons per time bin and selected with $0.2 < S < 0.8$. Correction factors for *E* and *S* were determined based on these measurements[7, 50] (see Methods).

Figure S4 Subpopulation-specific nsFCS of the AGQ peptide measured without ZMW.

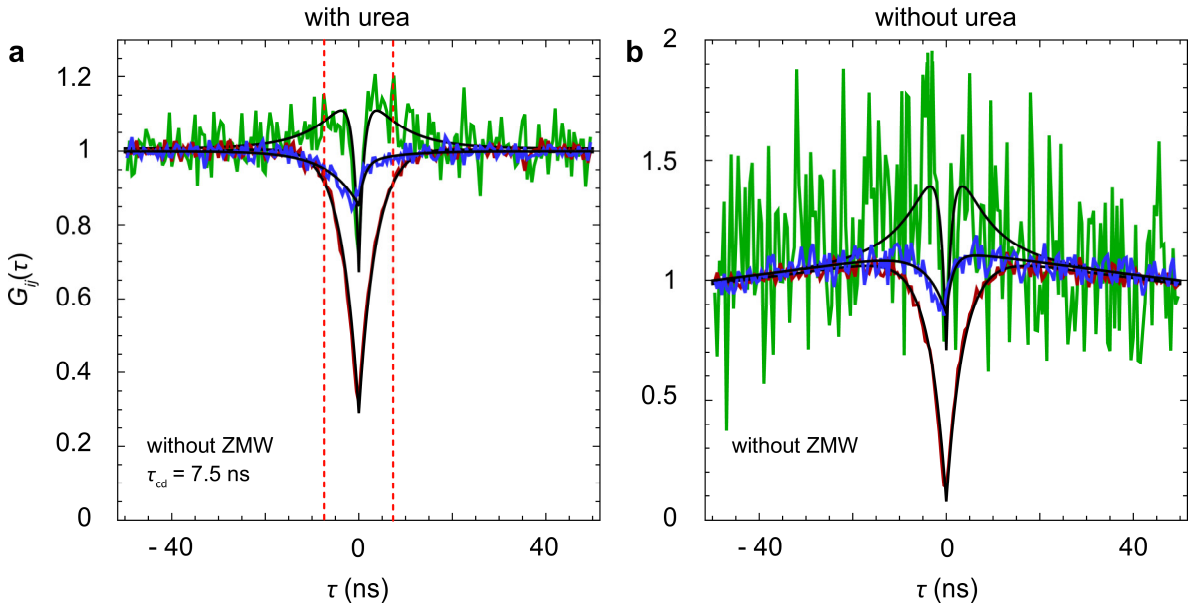

Overlay of donor (green) and acceptor (red) autocorrelations and donor-acceptor crosscorrelations (blue) for the AGQ peptide measured with 7.4 M urea (a) and without urea (b) with a linear binning of 500 ps. The fits (Eq. 8, see Methods) are shown as solid lines and require $\boldsymbol{\tau_{cd}}$, the relaxation time due to conformational dynamics, to be identical in all three correlations[28]. a, Correlation curves in the presence of urea show the signature of distance dynamics, with a positive amplitude in the donor autocorrelation and a negative amplitude in the acceptor-donor crosscorrelation, which is a prerequisite for unequivocally assigning this correlation signal to conformational dynamics[17]. The positive correlation in the acceptor autocorrelation, however, is undetectable owing to the overlap with the photon antibunching peak, illustrating the challenge of measuring dynamics with a timescale close to the fluorescence lifetimes of the dyes. $\boldsymbol{\tau_{cd}}$ is indicated as a red dotted line. (b) Correlation curves of the AGQ peptide measured without urea show no detectable contributions from conformational dynamics in the acceptor autocorrelation and in the acceptor-donor crosscorrelation owing to the overlap with the photon antibunching peak. The donor autocorrelation shows a positive amplitude with a decay time of ~5 ns. The pronounced noise in the donor autocorrelation is due to the high transfer efficiency (0.94) and correspondingly low donor photon detection rate. The fast dynamics observed without urea (4.2 ns) could only be resolved unequivocally with measurements in ZMWs, where the fluorescence lifetimes are reduced and the signal-to-noise ratio is increased (Figures 2d, S8). Note that in measurements without urea (b), the quenching from dye-dye stacking is detectable as an additional decay component on a timescale of ~220 ns in all three correlations. The asymmetry in the crosscorrelation functions is a consequence of the photophysics of the FRET process[47] (see Methods).

Figure S5. Subpopulation-specific nsFCS acquired from a mixture of AGQ peptide and ProTα measured with ZMW.

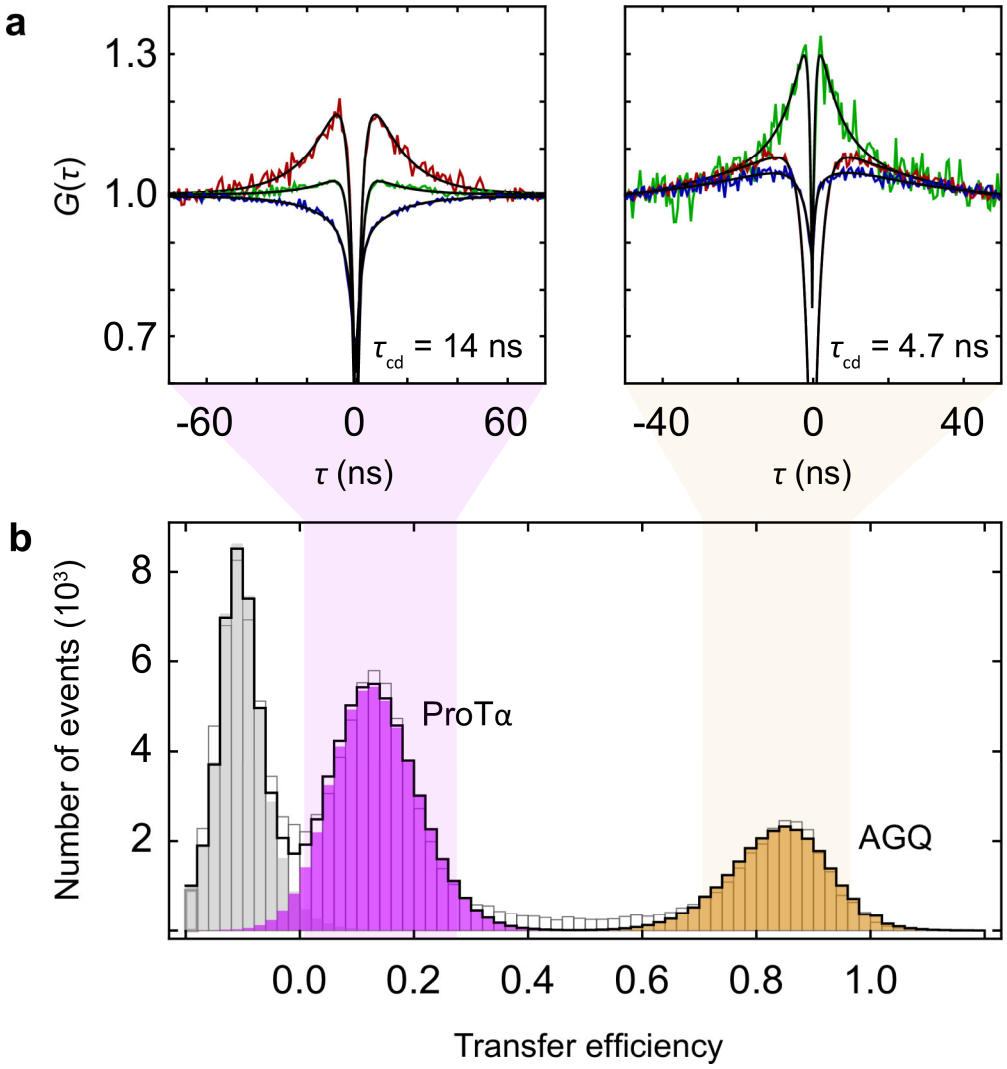

Subpopulation-specific nsFCS curves with a linear binning of 500 ps (a) and corresponding transfer efficiency histogram (b) from an 8-hour measurement in a ZMW using a mixture of the labeled AGQ peptide (orange) and ProTα[9] (purple) labeled with Alexa 488 and 594 at concentrations of 50 nM each, measured in 50 mM sodium phosphate, pH 7.4. (a) The fits (Eq. 8, see Methods) to the correlation data are shown as solid lines with the respective relaxation times, $\boldsymbol{\tau_{cd}}$, indicated.

Figure S6. ZMWs enable rapid data acquisition with nsFCS.

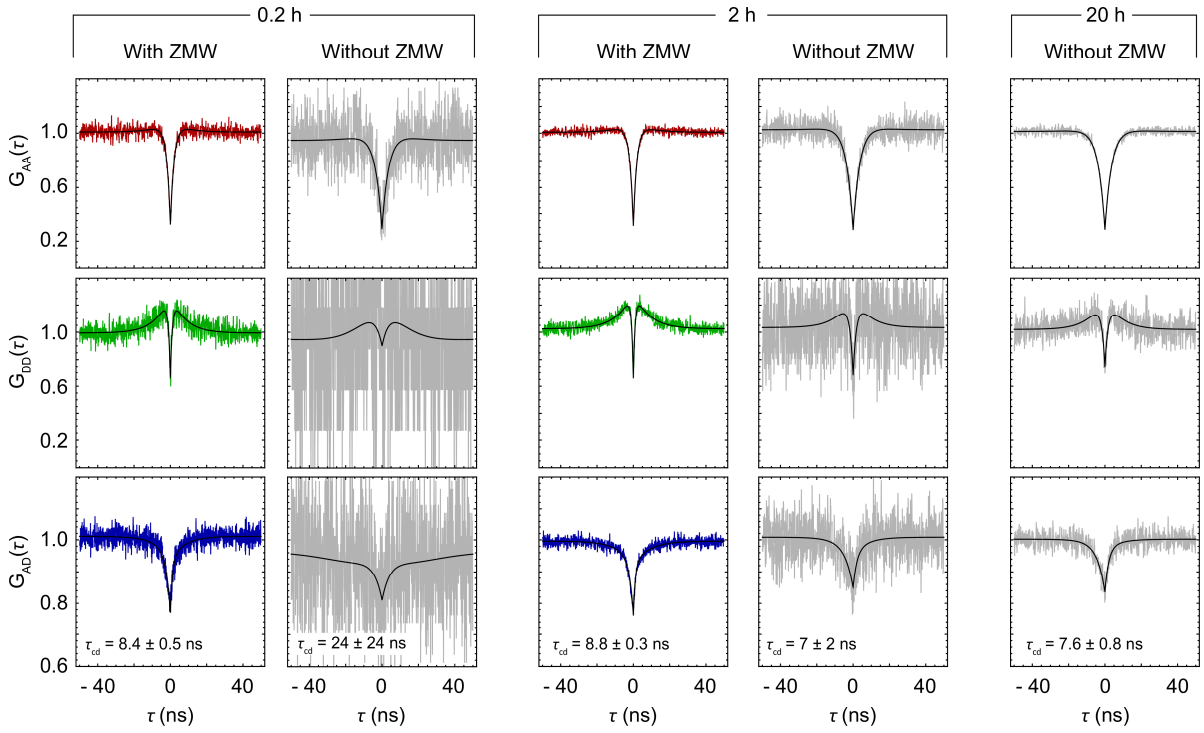

Comparison of donor autocorrelations (green), acceptor autocorrelations (red), and donor-acceptor crosscorrelations (blue) with a time binning of 100 ps for 0.2 h, 2.0 h, and 20 h of data acquisition (20 h only without ZMW), with resulting correlation times corresponding to conformational dynamics ($\boldsymbol{\tau_{cd}}$) and standard error from the global fit of all three correlations indicated in each column. Note the pronounced difference in noise between measurements with and without ZMW, especially for short acquisition times; as a result, $\boldsymbol{\tau_{cd}}$ obtained with ZMW is reliable already after ~0.2 h of data acquisition time, whereas $\boldsymbol{\tau_{cd}}$ obtained without ZMW is similarly reliable only after ~10-20 h. Correspondingly, the 0.2-h measurement with ZMW and the 20-h measurement without ZMW show comparable quality. Note the agreement of $\boldsymbol{\tau_{cd}}$ between measurements with and without ZMW, respectively, indicates that the presence of the nanostructure does not alter the peptide dynamics.

Figure S7. Convergence of all-atom MD simulations.

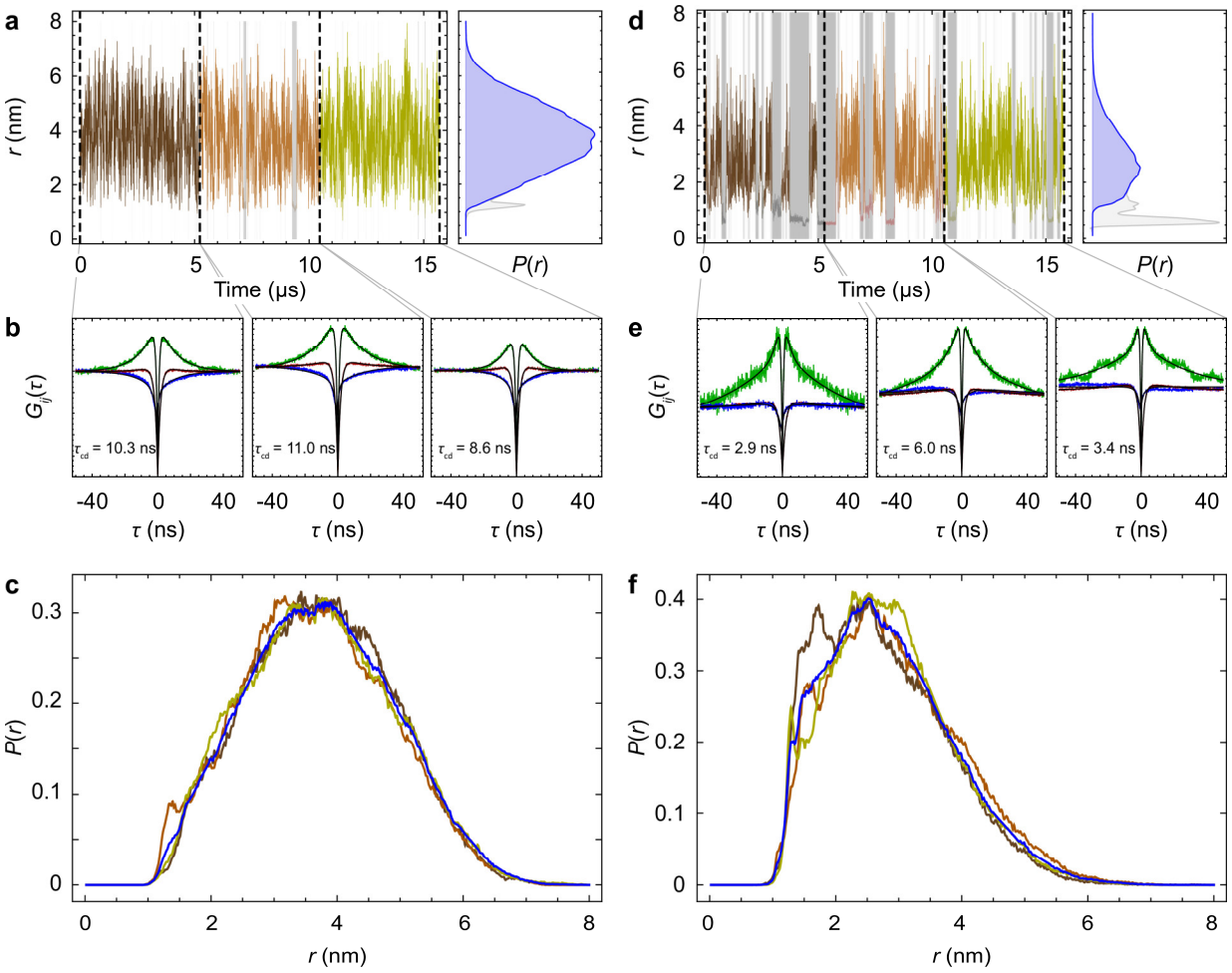

Concatenated time trajectories of the inter-dye distance, *r*, from 15 (a) or 17 (b) all-atom MD simulations (0.96 to 1.21 μs each) of the AGQ peptide with urea (a) and without urea (d). Gray-shaded areas indicate configurations where any two atoms of donor and acceptor dye are closer than 0.4 nm; these configurations were treated as non-emissive for the calculation of transfer efficiencies and intensity correlation curves (b,e), since they are expected to lead to dye-dye quenching[42-43, 51] (see Methods). Distance distributions of all (gray) and emissive configurations only (blue) are shown to the right of (a) and (d). The parts of the simulations color-coded in brown, orange, and yellow, respectively, were used for block averaging to assess convergence. (b) Fluorescence intensity correlations of the different blocks with urea (b) and without urea (d). Black solid lines show fits with Eq. 8 (see Methods); the resulting correlation times caused by distance dynamics, $\boldsymbol{\tau_{cd}}$, are indicated in each panel, leading to averages ± standard deviations of (9 ± 2) ns and (4 ± 2) ns for the simulations with and without urea, respectively. (c) Distance distributions (color code according to trajectory segments in (a) and (d)) of emissive conformations with urea (c) and without urea (f). Blue histograms are averages over the entire sets of simulations.

Figure S8. Comparison of nsFCS measured in ZMWs and from all-atom MD simulations without urea.

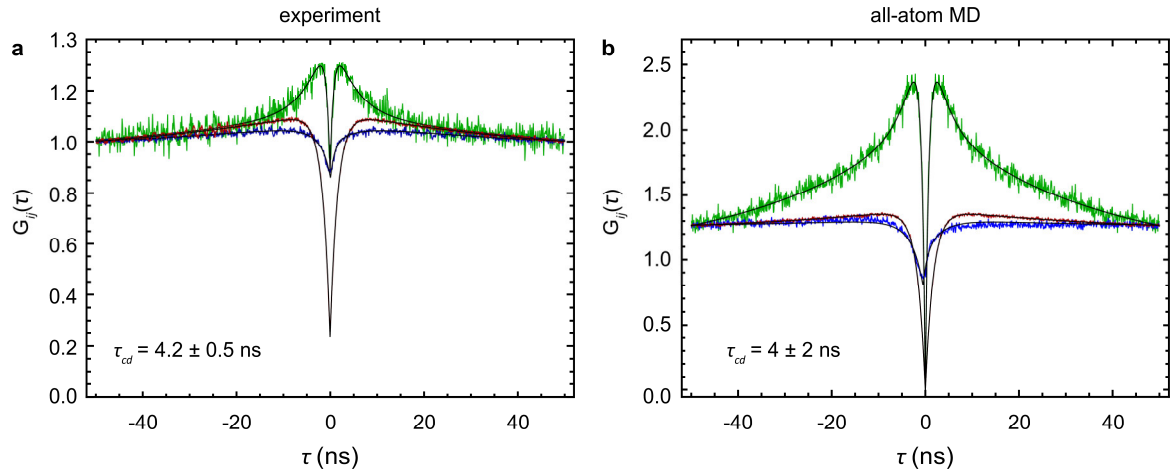

Direct comparison of measured (a) and simulated (b) correlation curves of the AGQ peptide measured without urea with global fits (solid black lines) (Eq. 8, see Methods) and resulting correlation times reporting on chain dynamics, $\boldsymbol{\tau_{cd}}$. The experimental error (a) is estimated from the standard deviation of 3 independent measurements; simulation errors are estimated analogously from block averaging using three simulation blocks of ~5 µs each (Figure S7). For the simulation of the correlation curves from the MD trajectories, conformations where any two atoms of donor and acceptor dye were within less than 0.4 nm were considered non-emissive owing to dye-dye quenching[42-43, 51] (Figure S7). Note that the additional slower decay component is more pronounced in the simulations than in the measurements, as reflected especially by the decay of the donor autocorrelation above ~10 ns, implying that dye interactions that slow down the dynamics are slightly overestimated in the force field. However, the value of $\boldsymbol{\tau_{cd}}$ in the 4-ns range can still be identified owing to the separation of timescales.

Figure S9. Surface passivation and sample stability in ZMWs.

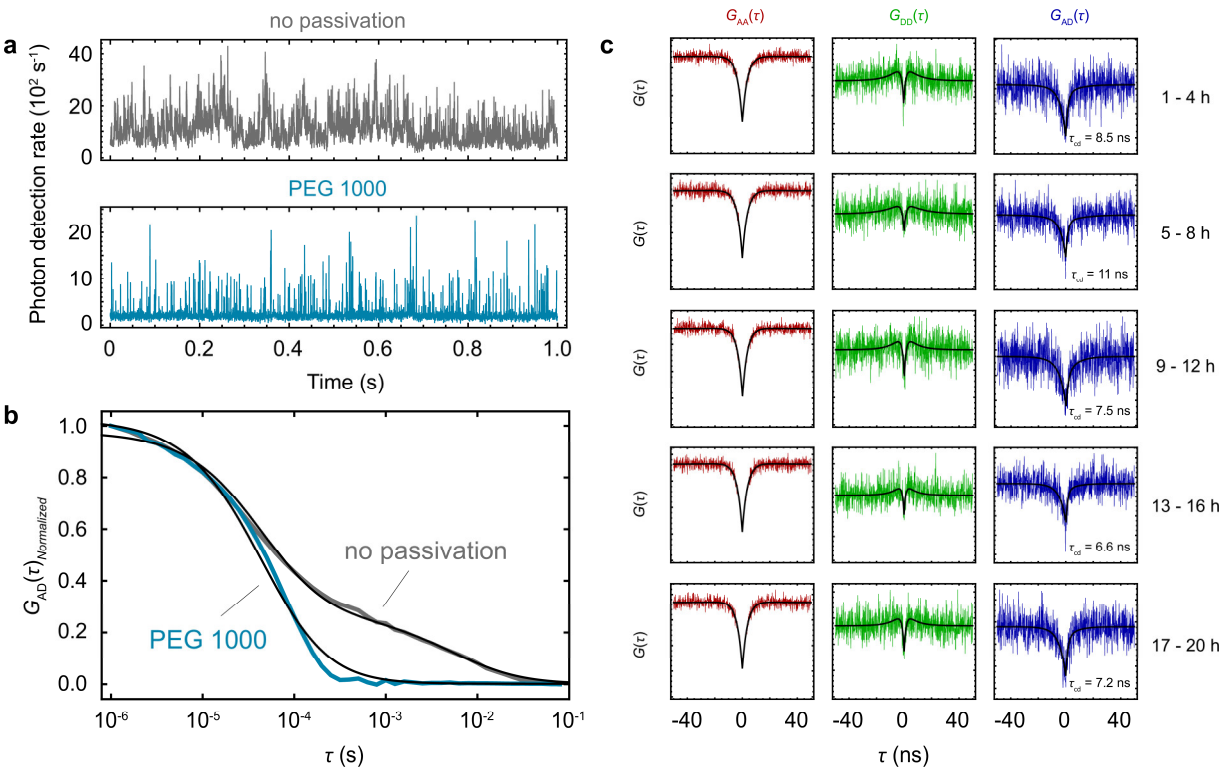

Fluorescence time traces of all detected photons (0.2-ms binning) (a) and correlation curves (b) of the labeled AGQ peptide measured in a non-passivated (gray) and a PEG-1000-passivated (blue) ZMW. The correlation curves were globally analyzed with a two-species model (Eq. 9, see Methods) to assess the relative amplitudes of the slow and fast diffusion components[1]. Without passivation, the relative amplitude of the slow diffusion component due to persistent surface interactions of the labeled AGQ peptide with the ZMW contributes 24 % to the correlation curve, whereas in the PEG-1000-passivated ZMW, no slow component could be detected. (c) Five 4-hour segments of donor (green) and acceptor (red) autocorrelations and donor-acceptor crosscorrelations (blue) for the AGQ peptide measured with 7.4 M urea with a linear binning of 100 ps. Fits (Eq. 8, see Methods) are shown as solid lines with the respective relaxation time, $\boldsymbol{\tau_{cd}}$, indicated.

Table S1. Parameters used to calculate transfer efficiencies from all-atom MD simulations (R_0: Förster radius; τ_D: donor fluorescence lifetime in the absence of acceptor) and comparison of experimental (exp.) and simulated (sim.) average transfer efficiencies, $\langle E \rangle$.

	with ZMW (urea)	**with ZMW** (no urea)	**without ZMW** (urea)	**without ZMW** (no urea)
R_0 (nm)	4.56	4.71	5.24	5.40
τ_D (ns)	2.24 ± 0.02	2.31 ± 0.02	3.77 ± 0.02	3.85 ± 0.02
$\langle E \rangle$ (exp.)	0.73 ± 0.03	0.88 ± 0.03	0.82 ± 0.03	0.94 ± 0.03
$\langle E \rangle$ (sim.)	0.70 ± 0.01	0.86 ± 0.01	0.80 ± 0.01	0.92 ± 0.01

References:

(1) Patra, S.; Baibakov, M.; Claude, J. B.; Wenger, J., Surface passivation of zero-mode waveguide nanostructures: benchmarking protocols and fluorescent labels. *Sci Rep-Uk* **2020,** *10*.

(2) Punj, D.; Ghenuche, P.; Moparthi, S. B.; de Torres, J.; Grigoriev, V.; Rigneault, H.; Wenger, J., Plasmonic antennas and zero- mode waveguides to enhance single molecule fluorescence detection and fluorescence correlation spectroscopy toward physiological concentrations. *Wires Nanomed Nanobi* **2014,** *6*, 268-282.

(3) Baibakov, M.; Patra, S.; Claude, J. B.; Moreau, A.; Lumeau, J.; Wenger, J., Extending Single-Molecule Forster Resonance Energy Transfer (FRET) Range beyond 10 Nanometers in Zero-Mode Waveguides. *ACS Nano* **2019,** *13*, 8469-8480.

(4) Nettels, D.; Hoffmann, A.; Schuler, B., Unfolded protein and peptide dynamics investigated with single-molecule FRET and correlation spectroscopy from picoseconds to seconds. *J Phys Chem B* **2008,** *112*, 6137-46.

(5) Muller, B. K.; Zaychikov, E.; Brauchle, C.; Lamb, D. C., Pulsed interleaved excitation. *Biophys. J.* **2005,** *89*, 3508-22.

(6) Nettels, D.; Gopich, I. V.; Hoffmann, A.; Schuler, B., Ultrafast dynamics of protein collapse from single-molecule photon statistics. *Proc. Natl. Acad. Sci. USA* **2007,** *104*, 2655-2660.

(7) Kapanidis, A. N.; Laurence, T. A.; Lee, N. K.; Margeat, E.; Kong, X.; Weiss, S., Alternating-laser excitation of single molecules. *Acc. Chem. Res.* **2005,** *38*, 523-33.

(8) Holmstrom, E. D.; Holla, A.; Zheng, W.; Nettels, D.; Best, R. B.; Schuler, B., Accurate Transfer Efficiencies, Distance Distributions, and Ensembles of Unfolded and Intrinsically Disordered Proteins From Single-Molecule FRET. *Methods Enzymol.* **2018,** *611*, 287-325.

(9) Müller-Späth, S.; Soranno, A.; Hirschfeld, V.; Hofmann, H.; Rüegger, S.; Reymond, L.; Nettels, D.; Schuler, B., Charge interactions can dominate the dimensions of intrinsically disordered proteins. *Proc. Natl. Acad. Sci. USA* **2010,** *107*, 14609-14614.

(10) Sottini, A.; Borgia, A.; Borgia, M. B.; Bugge, K.; Nettels, D.; Chowdhury, A.; Heidarsson, P. O.; Zosel, F.; Best, R. B.; Kragelund, B. B.; Schuler, B., Polyelectrolyte interactions enable rapid association and dissociation in high-affinity disordered protein complexes. *Nat. Commun.* **2020,** *11*, 5736.

(11) Baibakov, M.; Patra, S.; Claude, J. B.; Wenger, J., Long-Range Single-Molecule Forster Resonance Energy Transfer between Alexa Dyes in Zero-Mode Waveguides. *Acs Omega* **2020,** *5*, 6947-6955.

(12) de Torres, J.; Ghenuche, P.; Moparthi, S. B.; Grigoriev, V.; Wenger, J., FRET Enhancement in Aluminum Zero-Mode Waveguides. *Chemphyschem* **2015,** *16*, 782-788.

(13) Antonik, M.; Felekyan, S.; Gaiduk, A.; Seidel, C. A., Separating structural heterogeneities from stochastic variations in fluorescence resonance energy transfer distributions via photon distribution analysis. *J Phys Chem B* **2006,** *110*, 6970-8.

(14) Nir, E.; Michalet, X.; Hamadani, K. M.; Laurence, T. A.; Neuhauser, D.; Kovchegov, Y.; Weiss, S., Shot-noise limited single-molecule FRET histograms: Comparison between theory and experiments. *Journal of Physical Chemistry B* **2006,** *110*, 22103-22124.

(15) Kalinin, S.; Felekyan, S.; Valeri, A.; Seidel, C. A., Characterizing multiple molecular States in single-molecule multiparameter fluorescence detection by probability distribution analysis. *J Phys Chem B* **2008,** *112*, 8361-74.

(16) Zheng, W. W.; Zerze, G. H.; Borgia, A.; Mittal, J.; Schuler, B.; Best, R. B., Inferring properties of disordered chains from FRET transfer efficiencies. *J. Chem. Phys.* **2018,** *148*.

(17) Schuler, B.; Soranno, A.; Hofmann, H.; Nettels, D., Single-Molecule FRET Spectroscopy and the Polymer Physics of Unfolded and Intrinsically Disordered Proteins. *Annu. Rev. Biophys.* **2016,** *45*, 207-31.

(18) Schuler, B.; Lipman, E. A.; Eaton, W. A., Probing the free-energy surface for protein folding with single-molecule fluorescence spectroscopy. *Nature* **2002,** *419*, 743-747.

(19) Warren, J. R.; Gordon, J. A., On the Refractive Indices of Aqueous Solutions of Urea. *J. Phys. Chem. A* **1966,** *70*, 297-300.

(20) Rasnik, I.; McKinney, S. A.; Ha, T., Nonblinking and long-lasting single-molecule fluorescence imaging. *Nat. Methods* **2006,** *3*, 891-3.
(21) Schuler, B., Application of single molecule Forster resonance energy transfer to protein folding. *Methods Mol. Biol.* **2007,** *350*, 115-38.
(22) Hanbury Brown, R.; Twiss, R. Q., Correlation between Photons in Two Coherent Beams of Light. *Nature* **1956,** *177*, 27-29.
(23) Zander, C.; Enderlein, J.; Keller, R. A., *Single Molecule Detection in Solution, Methods and Applications*. Wiley-VCH: Berlin, 2002.
(24) Baibakov, M.; Barulin, A.; Roy, P.; Claude, J. B.; Patra, S.; Wenger, J., Zero-mode waveguides can be made better: fluorescence enhancement with rectangular aluminum nanoapertures from the visible to the deep ultraviolet. *Nanoscale Adv* **2020,** *2*, 4153-4160.
(25) Wenger, J.; Gerard, D.; Aouani, H.; Rigneault, H.; Lowder, B.; Blair, S.; Devaux, E.; Ebbesen, T. W., Nanoaperture-Enhanced Signal-to-Noise Ratio in Fluorescence Correlation Spectroscopy. *Anal Chem* **2009,** *81*, 834-839.
(26) Gopich, I. V.; Szabo, A., Photon counting histograms for diffusing fluorophores. *J. Phys. Chem. B* **2005,** *109*, 17683-8.
(27) Soranno, A.; Buchli, B.; Nettels, D.; Cheng, R. R.; Muller-Spath, S.; Pfeil, S. H.; Hoffmann, A.; Lipman, E. A.; Makarov, D. E.; Schuler, B., Quantifying internal friction in unfolded and intrinsically disordered proteins with single-molecule spectroscopy. *Proc. Natl. Acad. Sci. U S A* **2012,** *109*, 17800-6.
(28) Gopich, I. V.; Nettels, D.; Schuler, B.; Szabo, A., Protein dynamics from single-molecule fluorescence intensity correlation functions. *J. Chem. Phys.* **2009,** *131*, 095102.
(29) Hillger, F.; Hanni, D.; Nettels, D.; Geister, S.; Grandin, M.; Textor, M.; Schuler, B., Probing protein-chaperone interactions with single-molecule fluorescence spectroscopy. *Angew Chem Int Edit* **2008,** *47*, 6184-6188.
(30) Koshioka, M.; Sasaki, K.; Masuhara, H., Time-Dependent Fluorescence Depolarization Analysis in 3-Dimensional Microspectroscopy. *Appl Spectrosc* **1995,** *49*, 224-228.
(31) Brooks, B. R.; Bruccoleri, R. E.; Olafson, B. D.; States, D. J.; Swaminathan, S.; Karplus, M., Charmm - a Program for Macromolecular Energy, Minimization, and Dynamics Calculations. *J Comput Chem* **1983,** *4*, 187-217.
(32) Best, R. B.; Hofmann, H.; Nettels, D.; Schuler, B., Quantitative Interpretation of FRET Experiments via Molecular Simulation: Force Field and Validation. *Biophys. J.* **2015,** *108*, 2721-2731.
(33) Best, R. B.; Zheng, W.; Mittal, J., Balanced Protein-Water Interactions Improve Properties of Disordered Proteins and Non-Specific Protein Association. *J. Chem. Theory Comput.* **2014,** *10*, 5113-5124.
(34) Berendsen, H. J. C.; Postma, J. P. M.; Vangunsteren, W. F.; Dinola, A.; Haak, J. R., Molecular-Dynamics with Coupling to an External Bath. *J. Chem. Phys.* **1984,** *81*, 3684-3690.
(35) Parrinello, M.; Rahman, A., Polymorphic Transitions in Single-Crystals - a New Molecular-Dynamics Method. *J. Appl. Phys.* **1981,** *52*, 7182-7190.
(36) Abraham, M. J.; Murtola, T.; Schulz, R.; Páll, S.; Smith, J. C.; Hess, B.; Lindahl, E., GROMACS: High performance molecular simulations through multi-level parallelism from laptops to supercomputers. *SoftwareX* **2015,** *1-2*, 19-25.
(37) Zheng, W. W.; Borgia, A.; Borgia, M. B.; Schuler, B.; Best, R. B., Empirical Optimization of Interactions between Proteins and Chemical Denaturants in Molecular Simulations. *J Chem Theory Comput* **2015,** *11*, 5543-5553.
(38) Bussi, G.; Donadio, D.; Parrinello, M., Canonical sampling through velocity rescaling. *J. Chem. Phys.* **2007,** *126*.
(39) Darden, T.; York, D.; Pedersen, L., Particle Mesh Ewald - an N.Log(N) Method for Ewald Sums in Large Systems. *J. Chem. Phys.* **1993,** *98*, 10089-10092.
(40) Hess, B.; Bekker, H.; Berendsen, H. J. C.; Fraaije, J. G. E. M., LINCS: A linear constraint solver for molecular simulations. *J. Comput. Chem.* **1997,** *18*, 1463-1472.

(41) Gopich, I. V.; Szabo, A., Theory of the energy transfer efficiency and fluorescence lifetime distribution in single-molecule FRET. *P Natl Acad Sci USA* **2012,** *109*, 7747-7752.
(42) Vaiana, A. C.; Neuweiler, H.; Schulz, A.; Wolfrum, J.; Sauer, M.; Smith, J. C., Fluorescence quenching of dyes by tryptophan: Interactions at atomic detail from combination of experiment and computer simulation. *Journal of the American Chemical Society* **2003,** *125*, 14564-14572.
(43) Lapidus, L. J.; Eaton, W. A.; Hofrichter, J., Dynamics of intramolecular contact formation in polypeptides: Distance dependence of quenching rates in a room-temperature glass. *Phys. Rev. Lett.* **2001,** *8725*, 8101-+.
(44) Pochorovski, I.; Knehans, T.; Nettels, D.; Muller, A. M.; Schweizer, W. B.; Caflisch, A.; Schuler, B.; Diederich, F., Experimental and computational study of BODIPY dye-labeled cavitand dynamics. *Journal of the American Chemical Society* **2014,** *136*, 2441-9.
(45) Haenni, D.; Zosel, F.; Reymond, L.; Nettels, D.; Schuler, B., Intramolecular distances and dynamics from the combined photon statistics of single-molecule FRET and photoinduced electron transfer. *J. Phys. Chem. B* **2013,** *117*, 13015-28.
(46) Gopich, I. V.; Szabo, A., Theory of the statistics of kinetic transitions with application to single-molecule enzyme catalysis. *J. Chem. Phys.* **2006,** *124*, 154712.
(47) Nettels, D.; Haenni, D.; Maillot, S.; Gueye, M.; Barth, A.; Hirschfeld, V.; Hubner, C. G.; Leonard, J.; Schuler, B., Excited-state annihilation reduces power dependence of single-molecule FRET experiments. *Phys Chem Chem Phys* **2015,** *17*, 32304-32315.
(48) Rigneault, H.; Capoulade, J.; Dintinger, J.; Wenger, J.; Bonod, N.; Popov, E.; Ebbesen, T. W.; Lenne, P. F., Enhancement of single-molecule fluorescence detection in subwavelength apertures. *Phys. Rev. Lett.* **2005,** *95*, 117401.
(49) Barulin, A.; Claude, J. B.; Patra, S.; Bonod, N.; Wenger, J., Deep Ultraviolet Plasmonic Enhancement of Single Protein Autofluorescence in Zero-Mode Waveguides. *Nano Lett.* **2019,** *19*, 7434-7442.
(50) Hellenkamp, B.; Schmid, S.; Doroshenko, O.; Opanasyuk, O.; Kuhnemuth, R.; Rezaei Adariani, S.; Ambrose, B.; Aznauryan, M.; Barth, A.; Birkedal, V.; Bowen, M. E.; Chen, H.; Cordes, T.; Eilert, T.; Fijen, C.; Gebhardt, C.; Gotz, M.; Gouridis, G.; Gratton, E.; Ha, T.; Hao, P.; Hanke, C. A.; Hartmann, A.; Hendrix, J.; Hildebrandt, L. L.; Hirschfeld, V.; Hohlbein, J.; Hua, B.; Hubner, C. G.; Kallis, E.; Kapanidis, A. N.; Kim, J. Y.; Krainer, G.; Lamb, D. C.; Lee, N. K.; Lemke, E. A.; Levesque, B.; Levitus, M.; McCann, J. J.; Naredi-Rainer, N.; Nettels, D.; Ngo, T.; Qiu, R.; Robb, N. C.; Rocker, C.; Sanabria, H.; Schlierf, M.; Schroder, T.; Schuler, B.; Seidel, H.; Streit, L.; Thurn, J.; Tinnefeld, P.; Tyagi, S.; Vandenberk, N.; Vera, A. M.; Weninger, K. R.; Wunsch, B.; Yanez-Orozco, I. S.; Michaelis, J.; Seidel, C. A. M.; Craggs, T. D.; Hugel, T., Precision and accuracy of single-molecule FRET measurements-a multi-laboratory benchmark study. *Nat. Methods* **2018,** *15*, 669-676.
(51) Sauer, M.; Hofkens, J.; Enderlein, J., *Handbook of Fluorescence Spectroscopy and Imaging: From Single Molecules to Ensembles*. Wiley-VCH: Weinheim, 2011.